`


TRIBHUVAN UNIVERSITY

INSTITUTE OF ENGINEERING

PULCHOWK CAMPUS

**THESIS NO**: M-68-MSMDE-2020-2023

# Analysis of Bend Radius and Inlet Pipe Position on Hydronic Radiant Underfloor Heating System

by

Ishwor Acharya

A THESIS

SUBMITTED TO THE DEPARTMENT OF MECHANICAL AND AEROSPACE ENGINEERING IN PARTIAL FULFILLMENT OF THE REQUIREMENTS FOR THE DEGREE OF MASTER OF SCIENCE IN MECHANICAL SYSTEMS DESIGN AND ENGINEERING

DEPARTMENT OF MECHANICAL AND AEROSPACE ENGINEERING

LALITPUR, NEPAL

OCTOBER, 2023

`

## COPYRIGHT

`

**TRIBHUVAN UNIVERSITY**
**INSTITUTE OF ENGINEERING**
**PULCHOWK CAMPUS**
**DEPARTMENT OF MECHANICAL AND AEROSPACE ENGINEERING**

The undersigned certify that they have read, and recommended to the Institute of Engineering for acceptance, a thesis entitled **"Analysis of Bend Radius and Inlet Pipe Position on Hydronic Radiant Underfloor Heating System"** submitted by Ishwor Acharya in partial fulfillment of the requirements for the degree of Master of Science in Mechanical Systems Design and Engineering.

_____

Supervisor, Assistant Professor Dr. Sanjeev Maharjan
Department of Mechanical and Aerospace Engineering
Pulchowk Campus, Lalitpur

_____

External Examiner, Er. Manisha Maharjan
Senior Divisional Engineer (SDE)
Ministry of Education, Science and Technology

_____

Committee Chairperson
Assistant Professor. Dr. Sudip Bhattrai, PhD
Head, Department of Mechanical and Aerospace Engineering, Pulchowk Campus

Date: 06/10/2023

`


## ABSTRACT

A hydronic radiant underfloor heating system (RFHS) is a type of heating system that utilizes water as the heat transfer medium to provide comfortable and efficient heating in residential and commercial buildings. The rate of energy consumption on the household level for heating and cooling is increasing annually. Meeting future heating and cooling energy demand by alternative technology like floor heating systems (FHS) is a primary concern for engineers and designers. FHS has the advantages of lower investment cost, lower energy consumption, better thermal comfort, and maintaining the desired temperature up to human height. This merit has encouraged many researchers to study FHS in terms of temperature distribution, energy analysis, thermal analysis, and control strategy throughout the world. This study aims to investigate the effect of bend radius and change in the inlet position of pipe on temperature distribution over the floor surface for different mass flow rates. The findings of this analysis will provide valuable insights into the optimal bend radius, and temperature distribution which will provide improved design guidelines and recommendations for system installers, designers, and building professionals. In this study, a detailed investigation of a pipe embedded in a 75mm concrete floor was conducted, with a diameter of 13mm and pipe spacing of 150mm. The bottom of the floor was insulated, and various bend radii (ranging from 2mm to 190mm) were simulated to observe their impact on temperature near the bend. Three distinct piping layouts (offset serpentine, counterflow, and counterflow with a different inlet position) were designed using SolidWorks and simulated using Computational Fluid Dynamics (CFD) in ANSYS Fluent. When subjected to a mass flow rate of 0.23Lps, the counterflow layout had uniform temperature distribution of 309K on the floor surface. The offset serpentine layout exhibited a larger temperature drop on the floor surface compared to the counterflow layout. A comparison of the two layouts showed that the counterflow layout had lower pressure gradient and turbulent kinetic energy. The temperature near the bend region was influenced on changing the bend radius. Increasing the bend radius from 2mm to 30mm led to an increase in the temperature near the bend, while for bend radii above 40mm, the temperature near the bend region slightly decreased for a constant mass flow rate. Additionally, for the counterflow layout with change in inlet position, with a mass flow rate of 0.23lps, the temperature at the outlet was slightly higher, reaching 320K, and the overall temperature on the floor surface reached 310K.

`

## ACKNOWLEDGEMENT

I would like to express my sincere gratitude to Assistant Professor Dr. Sanjeev Maharjan for his valuable guidance, constant inspiration, and encouragement. His understanding of the subject matter and continuous support have been very important for the completion of the project. It was a great honor to pursue this project under his supervision. I would also like to express my due respect to the Department of Mechanical and Aerospace Engineering for their constant coordination and support.

My final thanks go to the faculty members, staff, and all our beloved friends of the Mechanical and Aerospace Engineering Department for their kind support and keen interest in the preparation of this thesis work.

I am grateful to all the department professors and lecturers for providing their precious suggestions and kind support throughout the project.

`

## TABLE OF CONTENTS

`

`

`

## LIST OF TABLES

`

## LIST OF FIGURES

`

## LIST OF SYMBOLS

| | |
|---|---|
| $\rho$ | Density |
| A | Area |
| $\sigma$ | Stratification coefficient |
| $C_p$ | Specific heat capacity |
| $\lambda$ | Thermal conductivity |
| h | Global heat transfer coefficient |
| $T_s$ | The floor surface average temperature |
| $T_m$ | The mean temperature |

`

## LIST OF ACRONYMS

| | |
|---|---|
| ASHRAE | American Society of Heating, Refrigerating, and Air Conditioning Engineers |
| CFD | Computational Fluid Dynamics |
| PEX | Poly Ethylene Cross-linked |
| PB | Polybutylene |
| LPS | Liters per second |
| RFHS | Radiant Floor Heating System |
| HVAC | Heating, Ventilation, and Air-Conditioning |

`

# CHAPTER ONE: INTRODUCTION

## 1.1 Background

Worldwide individuals and industries have enormous energy demand to power their homes, offices and to operate factories that produce substantial economic output. The buildings sector is a leading energy consumer which accounts for about 40% of the global energy consumption and contributes over 30% of the $CO_2$ emissions (Liu Yang et al., 2014). Despite the prevailing global energy crisis, a large amount of energy is consumed annually to maintain thermal comfort within buildings (Djamila, 2017). About 10% of energy consumption at the household level in Nepal is used for the heating and cooling sector (Sudhir Man et al., 2017)

Thermal comfort, as defined by the American Society of Heating, Refrigerating, and Air-Conditioning Engineers (ASHRAE), refers to the condition of mind that expresses satisfaction with the thermal environment. Both the hot and cold scenarios lead to discomfort. Achieving satisfaction with the thermal environment is essential as it has a direct influence on both productivity and health. Maintaining this standard of thermal comfort for occupants of buildings or other enclosures is one of the important goals for HVAC design engineers.

Hydronic RFHS work by circulating warm water through a network of pipes installed beneath the floor surface. The system consists of a heat source (such as a boiler or heat pump), a distribution system of pipes, and control mechanisms. These pipes are typically made of flexible, durable materials like cross-linked polyethylene (PEX) or polybutylene (PB). The pipes are laid out in a serpentine, counterflow pattern or in loops throughout the floor area, ensuring even heat distribution. FHS maintains desired indoor temperature through heat transfer between the radiant surface and room by conduction, convection, and radiation (H. Khorasanizadeh G.A, 2014). The floor surface radiates the heat upward, warming the objects, occupants in the room and maintaining the desired temperature.

RFHS has gained significant recognition as an effective and efficient method of heating in residential and commercial spaces. These systems utilize the principle of radiant heat transfer, where heat is emitted from a network of pipes or electric heating elements installed beneath the floor surface, providing comfortable warmth to the room. The use of RFHS in residential buildings is considerably more prevalent in the Nordic countries due to its thermal comfort benefits and efficient heating solution (Wang Y & Zhang X, 2018). In recent years, radiant underfloor heating has become increasingly popular in

`

residential and commercial buildings. The benefits of even heat distribution, energy efficiency, design flexibility, noise reduction and improved comfort have driven its adoption. The availability of different types of systems, including hydronic and electric, has expanded options for installation in various settings.

As technology and simulation capabilities continue to advance, researchers can gain valuable insights into the behavior of RFHS in various contexts, leading to better system designs, more sustainable and comfortable buildings.

### 1.2 Problem Statement

Hydronic RFHS has gained significant popularity due to its energy efficiency and comfortable heat distribution. Existing literature indicates that improper design choices, such as inadequate spacing, layout of heating pipes, suboptimal insulation, or inappropriate heat source sizing, can lead to uneven heat distribution, increased energy consumption, and reduced thermal comfort. Currently, there is a lack of comprehensive guidelines and design methodologies for floor heating systems installations, resulting in inconsistencies in system design and low performance. However, the design and installation of the FHS components play a crucial role in achieving optimal performance. Among these components, the bend radius of the pipe and inlet pipe position has been identified as critical factors that impact heat distribution and overall effectiveness.

Previous studies have compared different pipe layout configurations, such as serpentine and counterflow. These investigations aim to determine which layout provides the most even and efficient heat distribution across the floor surface. Researchers have explored the impact of pipe spacing and diameter on the performance of underfloor heating systems and how different pipe layouts impact the uniformity of heat distribution. However, research has lacked study on optimal pipe bend and position of inlet pipes which is a critical aspect of the study. The position of the inlets and the radius of the pipe bends can influence the temperature gradients within the underfloor heating system.

The choice of pipe bend radius and inlet position in FHS can lead to variations in flow rates and pressure distribution. This research aims to provide a thorough understanding of the fluid flow distribution, and heat distribution for offset and counterflow pipe layout. Uneven flow distribution may cause localized overheating or underheating in certain areas of the floor, affecting occupant comfort. Variations in pipe bend radius and inlet position can influence the heat transfer properties of the underfloor heating system.

`

Studying the effects of various bend radii and inlet positions, this study seeks to develop guidelines and recommendations for designing and installing hydronic RFHS that optimize efficiency, ensure uniform heat distribution, and enhance overall performance. By investigating the bend radius and inlet pipe position in hydronic radiant underfloor heating systems, this research aims to fill the existing knowledge gap and provide valuable insights for the design and optimization of these systems.

## 1.3 Objective

### 1.3.1 Main Objective

The main objective of this research is to analyze the bend radius and inlet pipe position on the hydronic radiant underfloor heating system.

### 1.3.2 Specific Objective

- To analyze the temperature distribution on the floor surface for offset serpentine and counterflow piping layout
- To analyze the pressure gradient, turbulent kinetic energy for offset serpentine and counterflow layout
- To analyze the temperature distribution near the bend for counterflow layout with bend radii 2mm,20mm,30mm,40mm,50mm,65mm, and 190mm
- To analyze the effect of inlet pipe position on temperature distribution for counterflow layout for different mass flow rate

## 1.4 Assumption and Limitation

The assumption and limitation of this research are listed as follows.

- Selective design parameters of the floor will be considered.
- Comparison of only three different piping layouts will be studied
- The research exclusively focuses on hydronic heating systems, while electrical resistance heating systems are not taken into consideration for analysis.
- Experimental validation of simulated results will not be performed
- Heat gain due to people and lightning have not been considered

`

# CHAPTER TWO: LITERATURE REVIEW

This chapter presents a brief review of the literature used throughout the thesis.

## 2.1 Thermal Comfort

Thermal comfort is that condition of mind that expresses satisfaction with the thermal environment (ASHRAE,2010). Because there are large variations, both physiologically and psychologically, from person to person, it is difficult to satisfy everyone in space. Various factors influence thermal comfort and occupants' subjective perception of their thermal environment. Air temperature is a primary factor that significantly affects thermal comfort. Studies by Humphreys and Nicol (2004) have highlighted the impact of indoor air temperature on occupants' thermal sensation and comfort. Relative humidity and air velocity also play important roles in thermal comfort. Research has shown that high humidity levels and low air movement can lead to discomfort (De Dear et al., 2018). Effective heating, ventilation, and air conditioning (HVAC) systems play a critical role in maintaining appropriate thermal conditions. Gao et al. (2017) reviewed HVAC system design approaches, emphasizing the importance of zonal control, air distribution, and energy-efficient technologies in maintaining thermal comfort.

## 2.2 Thermal conductivity

Thermal conductivity is a material property that quantifies its ability to conduct heat. It measures the rate at which heat flows through a substance per unit area, per unit thickness, and per unit temperature difference. Thermal conductivity indicates how well a material conducts heat and how quickly heat can move through it. Different materials have different thermal conductivities. Metals, such as copper and aluminum, have high thermal conductivity, while insulators like wood and plastic have lower thermal conductivity. Materials having high value of thermal conductivity indicates that it is good heat conductor, and a low value indicates that the material is a poor conductor or insulator.

Table 2.2: Thermal Conductivity of different materials

| Material | Thermal Conductivity, W/m°C |
|---|---|
| Concrete | 0.8 |
| Water | 0.607 |
| Crosslinked Polyethylene pipe | 0.47 |
| Mineral Wool | 0.042 |

`

### 2.3 Thermal diffusivity

Thermal diffusivity is a material property that characterizes how quickly heat diffuses through a material in response to a change in temperature. It quantifies the rate of heat conduction relative to the rate at which the material's temperature changes. In other words, thermal diffusivity represents how rapidly thermal energy spreads through a material in response to a temperature gradient.

$$\alpha = \frac{Heat\ Conduction}{Heat\ Storage} = \frac{k}{\rho \cdot \mathrm{Cp}}\ (\mathrm{m}^2/\mathrm{s})$$

where,

k is the thermal conductivity of material

$\rho$ represent material density

Cp represents the material's specific heat capacity at constant pressure

### 2.4 Radiant Underfloor Heating System

#### 2.4.1 Description

Radiant underfloor heating is a heating system that involves the installation of heating elements directly beneath the floor surface. RFHS operate by distributing heat through the floor surface, creating a comfortable and even warmth within a room. Warm water from the heat source (solar collector, boiler etc.) is distributed via a manifold to heating circuits made using pipes. The pipes are installed in a screed or timber floor. The floor area is typically warmed to 25°C to 30°C, providing an even distribution of heat at only slightly higher than room temperature.

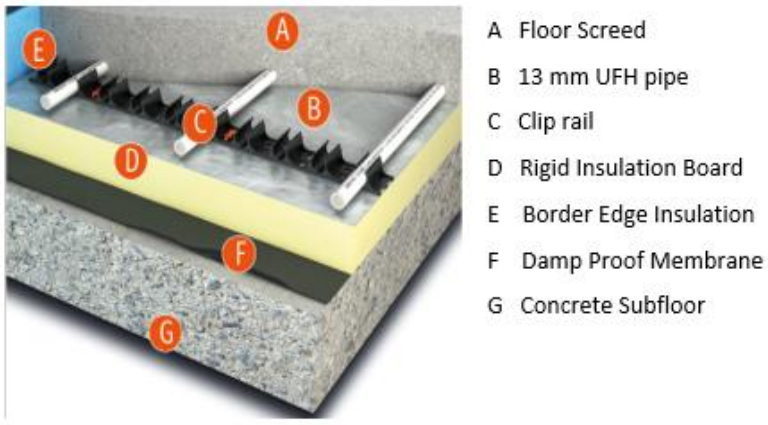


Figure 2.4.1 Underfloor Heating (Floor Heating Systems Guide, 2022)

`

### 2.4.2 Advantages of RFHS

Radiant underfloor heating systems offer several advantages

- **Comfort:** RFHS provides a high level of comfort by distributing heat evenly across the floor surface, creating a warm and comfortable environment. Unlike forced-air systems, which can create drafts and temperature variations, RFHS eliminates cold spots and provides consistent warmth throughout the room.
- **Energy Efficiency:** RFHS can be highly energy-efficient. They operate at lower water or electric temperatures compared to forced-air systems, resulting in reduced energy consumption. The radiant heat transfer from the floor surface directly warms the objects and occupants in the room, requiring less energy to maintain desired comfort levels.
- **Space-Saving Design:** RFHS eliminates the need for bulky radiators or baseboard heaters, freeing up wall space and providing more flexibility in interior design. Without the need for visible heating equipment, RFHS allows for a cleaner and more streamlined aesthetic.
- **Improved Indoor Air Quality:** RFHS does not rely on air circulation to distribute heat, reducing the movement of allergens, dust, and other airborne particles. This can help improve indoor air quality, making it a preferable option for individuals with respiratory sensitivities or allergies.
- **Quiet Operation**: RFHS operates silently, as there are no fans or blowers involved in heat distribution. This can create a more peaceful and serene environment compared to systems that generate noise during operation.
- **Longevity and Low Maintenance:** Radiant underfloor heating systems are known for their durability and low maintenance requirements. Properly installed systems can last for decades without the need for frequent repairs or replacements.

### 2.4.3 Types of RFHS

These systems typically use either hydronic (water-based) or electric heating elements installed beneath the floor.

- **Hydronic Radiant Underfloor Heating**

  Hydronic systems involve a network of pipes, often made of cross-linked polyethylene (PEX), installed in a serpentine or loop configuration beneath the floor. Heated water from a boiler or water heater is circulated through these pipes,

transferring heat to the floor. The warmed floor then radiates heat upward, providing a comfortable environment. Hydronic systems offer the advantage of being highly efficient, as water has a high thermal conductivity and can retain heat for longer periods.

Hydronic systems require skilled designers and trades people familiar with boilers, circulators, controls, fluid pressures and temperature. The use of modern factory assembled sub-stations, used primarily in district heating and cooling, can greatly simplify design requirements and reduce the installation and commissioning time of hydronic systems.

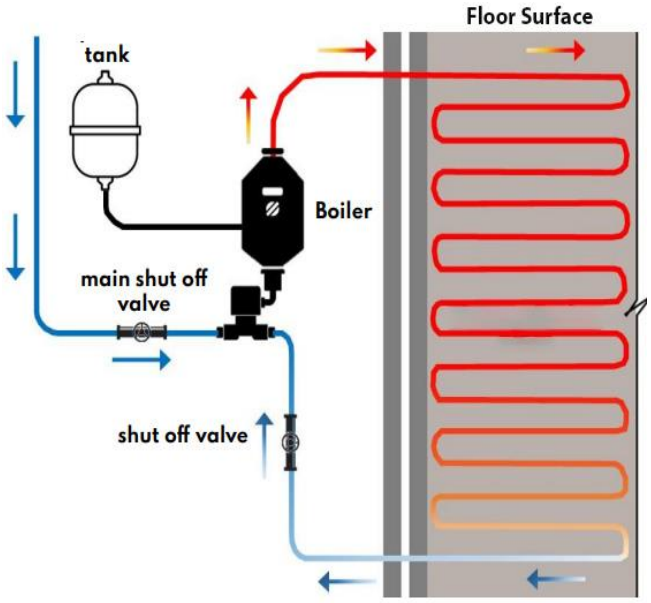


Figure 2.4.3: Hydronic Radiant Underfloor Heating (Floor Heating Guide, 2022)

- **Electric Radiant Underfloor Heating**

  Electric systems utilize electric heating elements, such as cables or mats, installed beneath the floor surface. When an electric current passes through these elements, they generate heat, which is then transferred to the floor. Electric systems are easier to install and do not require a separate heat source like boilers. They provide precise temperature control and can be zoned for individual room control.

  Electric systems have a simpler installation and commissioning process with fewer components compared to hydronic systems. Certain electric systems employ line voltage technology, while others utilize low voltage technology. Electric underfloor heating systems are compatible with a wide range of flooring materials, offering versatility and adaptability to different interior styles.

`

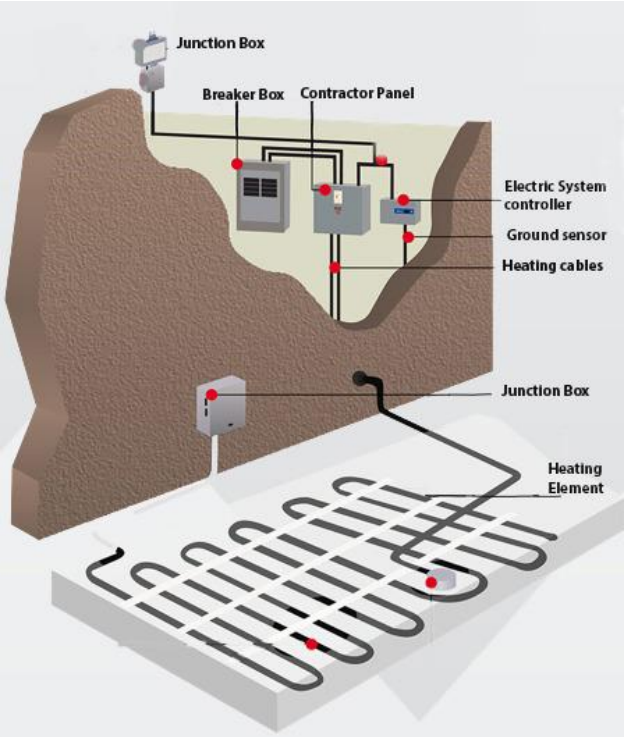


Figure 2.4.4: Electric underfloor heating system (Floor Heating Guide, 2022)

- **Air Heated Radiant Underfloor Heating System**

  Air-heated systems represent the earliest form of radiant heat, initially employed in China, Korea, and Rome. These systems are somewhat less effective than other types and are consequently less widespread. Instead of directly pumping heated air beneath the floor, the warm air circulates through a network of tubes, resembling the way water is utilized.

## 2.5 Types of Floor construction

Radiant floor heating systems can be installed in various types of floor constructions. The suitability of each construction type depends on factors such as the system's heat output, the type of building, and the desired floor covering

### 2.5.1 Screed or Solid Floor

This type of construction involves pouring a concrete slab directly on the ground. Radiant heating tubes or cables are embedded within the slab, which acts as a thermal mass, providing consistent and efficient heat distribution.

`

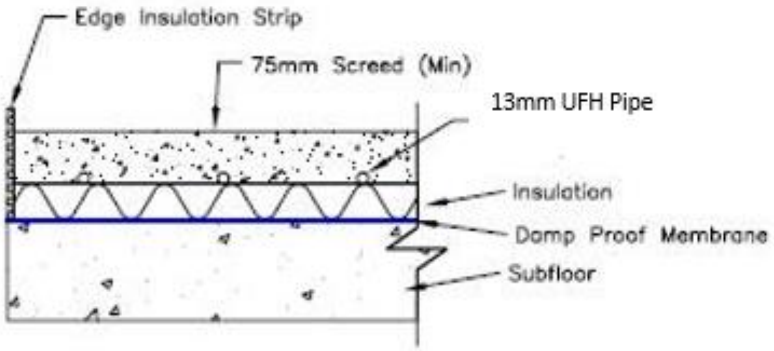


Figure 2.5.1: Solid Floor Construction (Joy Plumbing Limited, 2017)

### 2.5.2 Thin Slab

Thin slab construction involves pouring a thinner layer of concrete (around 1 inch to 2 inches thick) over a subfloor or insulation board. The radiant heating system is embedded within this thin layer of concrete.

### 2.5.3 Suspended Slab

A suspended slab is a type of floor construction where the heating system is installed within the void between the structural floor and the finished floor surface. This method is commonly used in both residential and commercial buildings to provide comfortable and efficient heating. The suspended slab consists of a reinforced concrete slab that is supported by beams, columns, or walls. The structural members (beams and columns) provide the necessary support for the weight of the slab and any additional loads, such as furniture, occupants, or equipment.

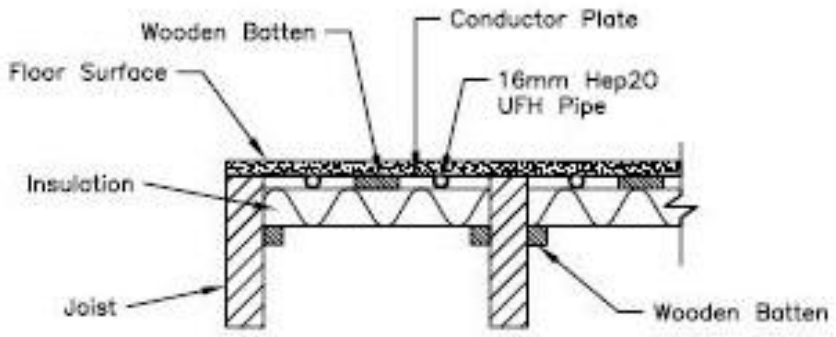


Figure 2.5.3 Suspended Floor Construction (Joy Plumbing Limited, 2017)

`

## 2.6 Types of Piping

### 2.6.1 Single Serpentine

The simplest layout option is the single serpentine. In this design, a single pipe enters the room and uses a ‘zig-zag’ motion to span the length of the room. The pipe then exits through the entry point. The hot water which enters the room gradually cools as it runs through the system. At the entry point, the system has a higher heat output, and the room therefore becomes cooler at one end. By using a serpentine layout, the heating elements can be evenly spaced and positioned to prevent any cold spots in the floor.

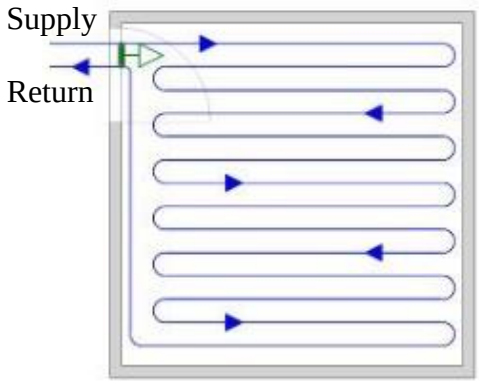


Figure 2.6.1 Serpentine Pipe Layout (Central Heating Guide,2019)

### 2.6.2 Double Serpentine

In a double serpentine layout, the pipe enters and runs along the perimeter of the room, before creating a ‘zig zag’ layout, then running back on itself to create a contraflow. The cooler water, therefore, runs alongside the warmer water nearer to the pipe entrance, allowing the temperature to ‘even out’ throughout the room. This is an effective method to create a more even distribution of heat, however, it can’t be used with plated systems.

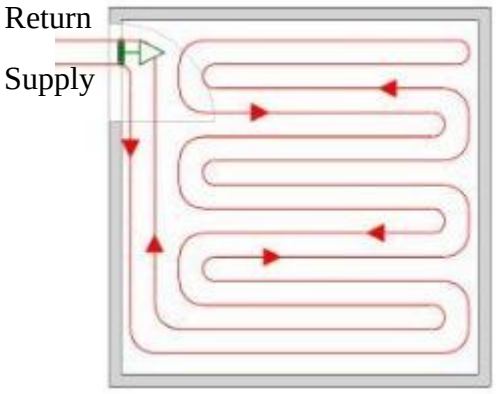


Figure 2.6.2 Double Serpentine Pipe Layout (Central Heating Guide,2019)

`

### 2.6.3 Concentric Layout

A concentric layout underfloor heating system refers to a specific configuration of pipes or heating elements used to distribute warmth evenly beneath the floor surface in a building. The concentric layout simplifies the installation process since the loops can be arranged in a continuous and organized manner. The pipe is run around the perimeter of the space, then repeatedly tracked around the room, creating a spiral shape, before reaching the center. The pipes deliver the most heat around the outskirts of the room, where heat naturally escapes, while the center of the room is heated the least by the system.

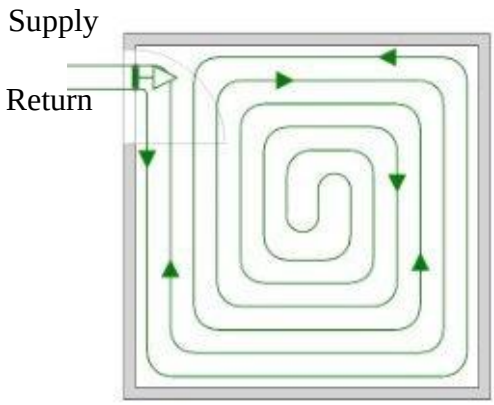


Figure 2.6.3 Concentric Pipe Layout (Central Heating Guide,2019)

## 2.7 Important Design Parameters

When designing a radiant floor heating system, several important parameters should be considered to ensure optimal performance. Designing a floor heating system requires careful consideration of various parameters to ensure optimal performance, energy efficiency, and occupant comfort. Here are some important design parameters to take into account:

### 2.7.1 Floor Covering Selection

The choice of floor covering can impact the system's performance. Floor coverings have different thermal conductivities and resistance to heat transfer. It is important to consider the thermal properties of the flooring material to ensure efficient heat transfer from the radiant system to the room.

### 2.7.2 Tube Size

The tube size directly influences the heat output capacity of the system. Larger diameter tubes can carry more water, which results in higher heat output. The tube size impacts the required flow rate of the heated water and influences the pressure drop within the system. Proper tube sizing is essential to achieve even heat distribution across the floor surface

`

### 2.7.3 Tube Depth

Tube depth must be carefully chosen to achieve optimal heat transfer and avoid excessive heat loss. Installing the tubes too close to the floor surface may lead to uneven heat distribution and "hot spots," while installing them too deep may reduce the system's efficiency and response time. The proper tube depth is essential to ensure effective heat transfer and even distribution of warmth across the floor surface.

### 2.7.4 Tube Spacing and Layout

The spacing and layout of the radiant heating tubes or cables affect the heat distribution across the floor surface. Proper tube spacing is crucial to ensure uniform heating without hot or cold spots. Factors such as the heat output, room size, and floor covering influence the appropriate tube spacing.

### 2.7.5 Thermal Insulation

Insulation beneath the radiant floor system helps minimize heat loss downwards, ensuring efficient heat transfer upwards into the room. Proper insulation selection and installation reduce energy consumption and improve system performance. Insulation materials with high R-values are commonly used to minimize heat loss

## 2.8 Review of Past Researches

Understanding how radiant heating systems perform under various conditions is vital, and comprehensive simulations are currently being conducted to gain deeper insights into their behavior. A significant advancement in radiant floor heating occurred with the adoption of Polyethylene (PEX) tubes, marking a major milestone as it effectively resolved issues associated with older pipe materials.

Underfloor heating is a method that uses pipes placed in the floor to distribute heat in both vertical and horizontal directions by circulating hot water (Hasan et al., 2013). The practice of warming and cooling floors in structures began as a traditional European method more than thirty years ago. In recent times, it has gained popularity in numerous countries and is extensively applied in homes and public buildings. Economically, this system can deliver warmth with lower energy consumption, along with enhanced control, efficiency, and quality (Xiaozhou et al., 2015).

Studies in the 1960s and 1970s, such as those by Eickhoff and Liu, investigated the heat transfer characteristics of radiant floor heating systems using different pipe materials and

`

configurations. They investigated the heat distribution patterns in radiant panel floors and understand the factors influencing the thermal performance of these systems. The findings of the study indicated that the heat distribution in radiant panel floors is influenced by various factors, including the spacing between the heating elements, floor covering materials, and insulation. Eickhoff observed that closer spacing between the panels resulted in more uniform temperature distribution and improved thermal comfort. The study also highlighted the importance of proper insulation to minimize heat losses and enhance system efficiency.

Early research by Banerjee and Palmer (1991) examined the effect of pipe spacing and insulation on the performance of radiant underfloor heating. They found that increasing pipe spacing reduced the energy consumption of the system while maintaining thermal comfort. The researchers observed that the spacing between the heating pipes significantly influenced the temperature distribution and system performance. The study also highlighted the importance of insulation beneath the floor surface to minimize heat

Gao et al. (2018) investigated five distinct layouts for underfloor heating pipes. The center spacing intervals varied from 300 mm to 500 mm, and the supply water temperature was set at 50 °C. The study assessed the even distribution of heat across the floor and variations in vertical air temperature gradients. The results indicated that the system maintained a consistent indoor air temperature field above 0.1 m from the floor, with a temperature difference not exceeding 1 °C. The study concluded that the optimal layout for the under-floor heating pipe is with a center spacing of 400 mm.

Significant emphasis is placed on RFHS research to discover the most suitable choices for design, construction, and control, with the ultimate goal of establishing it as a financially viable heating solution for commercial buildings in the future. According to reports, there has been a 36% increase in the number of commercial radiant system specifications since 2005. Additionally, approximately 7.5% of new constructions now include radiant systems in their specifications, and this percentage is expected to grow significantly shortly. (ASHRAE Journal 52).

Liu & Li, (2015) did detailed investigation into the thermal performance and energy efficiency of two different piping layouts for underfloor heating systems: serpentine and counterflow configurations. The findings demonstrated that both layouts are capable of delivering efficient and effective heating to indoor spaces. The serpentine layout showed

`

satisfactory thermal performance, effectively heating the floor surface and providing a comfortable indoor environment. On the other hand, the counterflow layout exhibited superior thermal performance compared to the serpentine layout. The numerical simulations revealed that the counterflow layout achieved more uniform heat distribution across the floor surface.

In a study conducted by Wang in 2014, the impact of three different heating methods on the indoor airflow thermal performance of a residential building was investigated using simulations. Three physical models representing residential rooms heated with radiators, air conditioners, and floor heating were created. Three-dimensional numerical simulations were conducted to analyze the temperature field, velocity field, and pressure field, and cloud maps and vector diagrams were used for analysis. The findings revealed that floor heating provides a more uniform temperature field and lower air flow velocity compared to the other heating methods (radiators and air conditioners). As a result, floor heating offers better thermal comfort in the room.

ASHRAE (2017) recommends a maximum floor surface temperatures of 29℃ in occupied-spaces for comfort reasons in terms of overheating. The air temperature could range from between approximately 19.4℃ to 27.8℃.

Numerous numerical and experimental studies were conducted over the past few decades to learn more about the thermal behavior of FHS. Ngo et al., (2015) conducted a study which investigated the effect of design parameters on the performance of a radiant floor heating system. The experiment involved testing different pipe spacings (4 to 12 inches), depths (2.5 to 6.5 inches), and temperatures (45°C, 65°C, and 85°C) in three different mediums (air, gravel, and sand). The results showed that the most desirable floor temperature distribution was achieved with a shallow burial depth and closer pipe spacing. For instance, at a pipe spacing of 4 inches and depth of 2.5 inches, the floor surface temperature was relatively uniform, with a variation of only 1.6°C. The study also found that the average floor temperature was higher when the piping system was embedded in an air-filled space than in a porous medium such as gravel or sand.

There have been several studies examining the RFHS using different mathematical models such as the finite volume method (FVM), finite difference method (FDM), and finite element method (FEM). Jin et al. (2010) specifically focused on using the finite volume method to investigate the performance of a RFCS by analyzing the impact of

`

resistance to heat flow and velocity of water. Their findings indicated that a lower thermal conductivity of the pipe is crucial for optimal system performance. Additionally, they found that water velocity has a minimal effect on the heat exchange between the water and the slab.

Recent research has focused on integrating radiant underfloor heating systems with renewable energy sources, such as solar thermal and geothermal systems. These initial research studies have provided valuable insights into the principles, performance, and optimization of radiant underfloor heating systems. They have laid the groundwork for further advancements in the field, fostering energy-efficient and comfortable heating solutions for buildings. The underfloor heating was modelled and simulated for two alternative pipe configurations serpentine and counterflow by Sarika Kumar Mishra, 2017. The simulation results demonstrated the spiral loop's efficiency and ability to achieve a uniform temperature distribution. Further their research advised to use the low value of pipe spacing and larger radius bends during installation as the space between pipe bends was identified to be crucial.

In addition to exploring design guidelines for heating systems, extensive research has been conducted on various aspects of underfloor heating systems. These include investigating different types of flooring, examining thermal storage options, and studying various piping materials. Research has focused on comparing different pipe materials, such as PEX, PB, copper, and composite pipes, in terms of thermal conductivity, durability, and compatibility. Understanding the impact of pipe material on heat transfer efficiency and system response time is crucial for optimizing underfloor heating systems. Studies have examined the heat transfer characteristics, temperature distribution, and energy efficiency of underfloor heating systems. Factors such as pipe spacing, flow rates, insulation, and control strategies have been investigated to enhance system performance and energy conservation. The findings from relevant studies consistently indicate that underfloor heating is an effective and highly researched method for space heating worldwide.

`

## CHAPTER THREE: RESEARCH METHODOLOGY

The research methodology of the research work is presented in Figure 3.1. Different task carried out for accomplishment of the study is mentioned in the methodology. This research is also carried out in the sequential order. Initially started with research topic, objectives, literature review, model simulation and ended with documentations and publications.

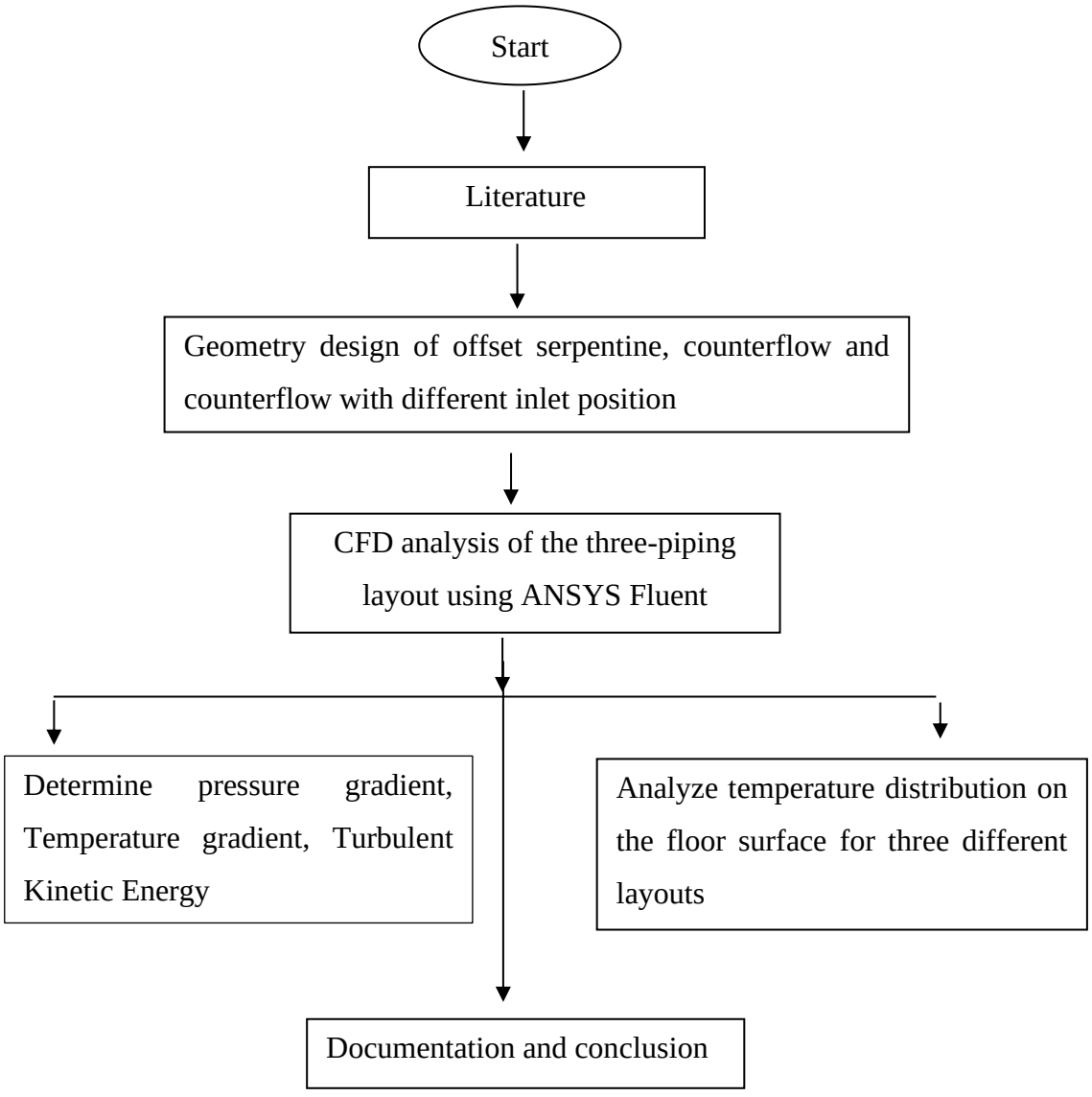


Figure 3.1: Research Methodology

`

For this study different articles, journals, publications, books and other sources were consulted. Based on this the radiant floor heating topic was finalized and objectives were set up. As, floor heating is inseparable part of HVAC design, many articles related to it were available. The research documents which are closely related to our topic of interest and synchronizing with our objectives are shortlisted and reviewed for the guidance for this research to be carried out smoothly.

### 3.1 Literature Review

The research works in the related topic of Radiant Floor Heating are collected from various sources. These researches are then reviewed to identify the problem statement. Other literary researches are reviewed in order to find a suitable solution to the research gap identified.

### 3.2 Geometry design and Model Description

Three different piping layout offset serpentine, counter flow and counterflow with different inlet position were designed in the solid works. The geometry is designed with larger radius of bend for both counterflow and offset serpentine layout as recommended by S.K Mishra, 2017. Several piping layouts with different bend radii 2mm,10mm,20mm,30mm,40mm,50mm,65mm,190mm were also designed. The offset serpentine, counterflow layout and counterflow with different inlet position are discussed in following sections.

#### 3.2.1 Geometry design for Offset Serpentine Layout

The offset serpentine piping layout, designed on an 11.89$m^2$ floor with dimensions 4.75m × 2.50m × 0.075m, is depicted in figure 3.2.1 (a) below. This layout employs a continuous pattern across the floor space, with pipes vertically offset at a distance of 20mm from their centers. One pipe is placed below the other, with a 5mm gap between their surfaces. The primary objective of this layout is to accommodate larger bend radii. The design features one side with a larger bend radius of 230mm, while the opposite side has a shorter bend radius of 75mm. Each pipe has a diameter of 13mm and is spaced at a distance of 150mm from the next. In total, 80m of pipe is used for this model. The inlet and outlet are located at the bottom of the floor, spaced 150mm apart. Specifically, the inlet position is 150mm from the bottom edge of the concrete floor. The pipes feature 15 bends from the bottom to the top, positioned 12mm above the floor's bottom, as shown in Fig (a) section E-E. Additionally, the bend pipes are spaced 150mm from the floor edges. To ensure thermal efficiency, the bottom of the floor is equipped with 25mm of insulation.

`

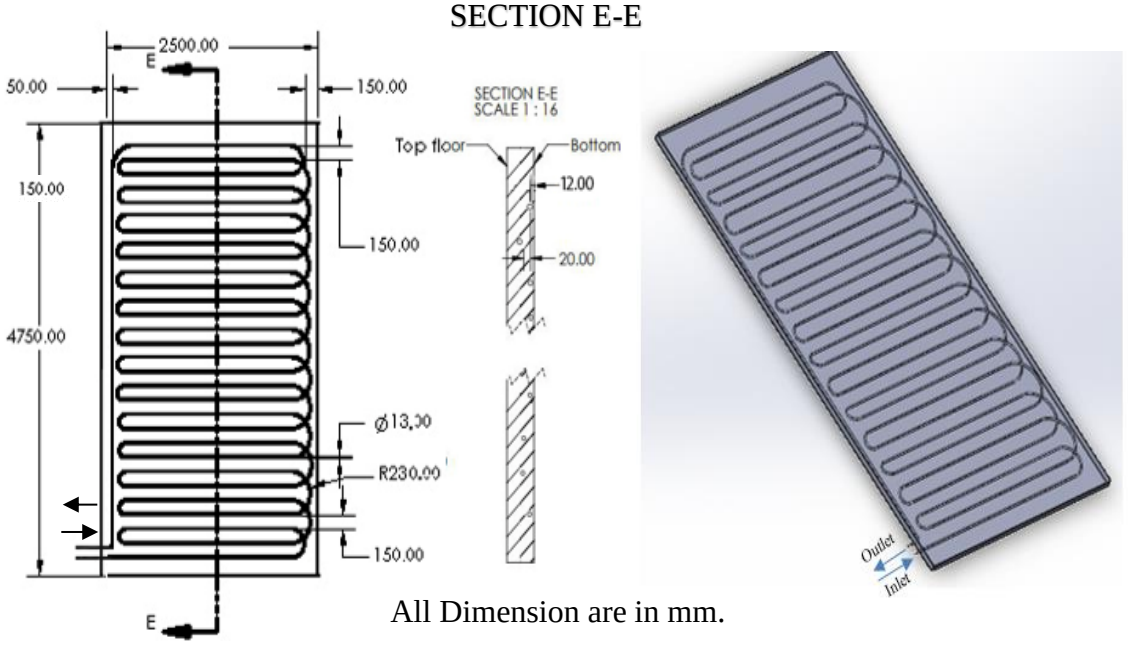


All Dimension are in mm.

(a) 2D drawing of Offset Serpentine Floor and piping layout

(b) 3D drawing of Offset Serpentine floor and piping layout

Figure 3.2.1: Offset Serpentine 2D and 3D drawing

### 3.2.2 Geometry design for Counterflow layout

In a counterflow layout configuration, the piping system is organized such that adjacent loops have opposite directions of water flow. This means that if one loop has water flowing clockwise, the next adjacent loop would have water flowing counterclockwise. The counterflow layout is designed on a floor with an area of 11.89m$^2$, featuring a bend radius of 190mm, a diameter of 13mm, and a length of 80m. The pipe is embedded 12mm above the bottom surface of the concrete floor. Both the inlet and outlet are located at the bottom of the floor, positioned 150mm from the floor edge. A total of 7 pipe circuits are used in this layout, with a consistent spacing of 150mm throughout the floor surface. To enhance thermal efficiency, the bottom of the floor is insulated with a layer of 25mm.

`

`

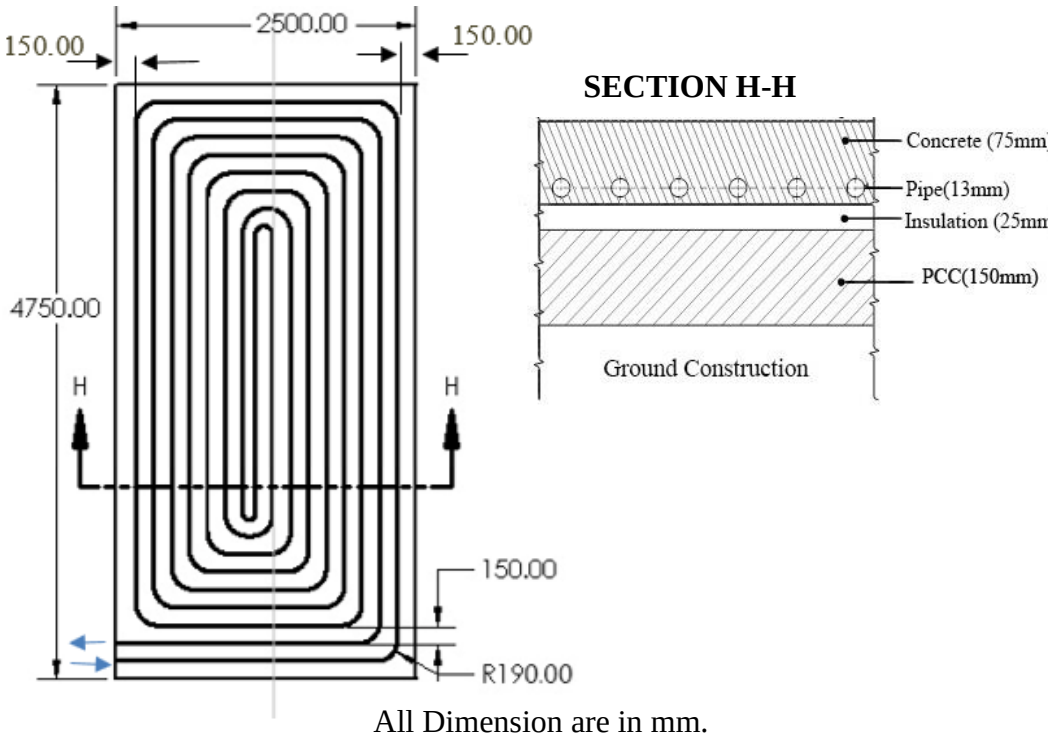


All Dimension are in mm.

(a) 2D drawing of counterflow Floor and piping layout


(b) 3D drawing of counterflow Floor and piping layout

Figure 3.2.2: Counterflow layout 2D and 3D drawing

`

### 3.2.3 Geometry design for Counterflow with different inlet position

The counterflow layout with different inlet positions, illustrated in figure 3.2.3 (a), is designed on a floor with dimensions 4.75m × 2.50m × 0.075m. This layout has an area of 11.89m2 and features a bend radius of 30mm and a pipe diameter of 13mm. The pipes are embedded 12mm above the bottom surface of the concrete floor, with a consistent spacing of 150mm throughout the floor surface. The total length of pipe used in this model is 80m, and the inlet is positioned at 1150mm from the bottom edge of the floor, with a spacing of 150mm from the outlet. The layout comprises 7 pipe circuits, and the bottom of the floor is equipped with a 25mm insulation layer. In the layout shown in figure (a), the inlet is centrally positioned, and the pipes run outward from the center. Here, the fluid initially flows towards the center of the floor, then moves outwards towards the corners of the floor, flows back towards the center, and eventually exits through the outlet.

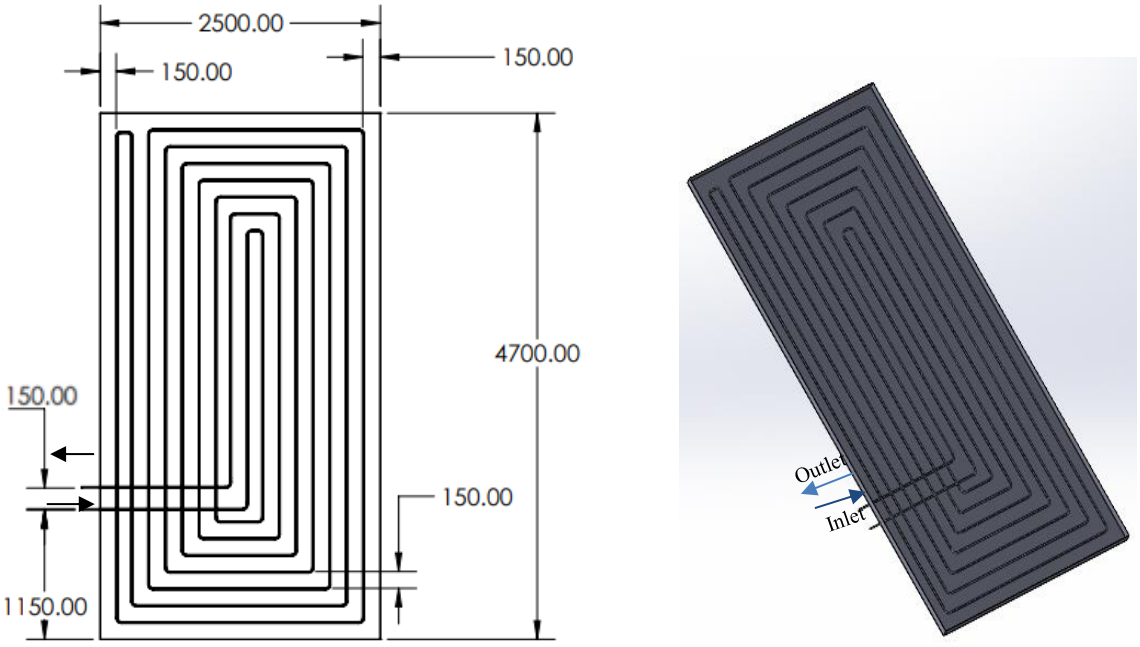


All Dimension are in mm.

(a) 2D drawing of Counterflow Layout (b) 3D design of Counterflow Layout

Figure 3.2.3: Counterflow with different inlet position 2D and 3D drawing

`

### 3.3 Finite Element Model

#### 3.3.1. Governing equations

To simulate the performance and the real interaction between the under-floor heating system and the floor surface, a numerical simulation is conducted with the commercial Computational fluid dynamics (CFD) code Fluent which is based on finite volume method.

In order to simplify the numerical simulation model of the under-floor heating system, the theoretical heat transfer models are expressed by the following assumptions:

- The thermal properties of the system panel are isotropic and independent of temperature.
- Temperature gradients of the solid region where pipes embedded are also considered in the analysis.
- Water was used as a working fluid.
- Based on the investigated mass flow inside pipes, the flow is turbulent. All simulations are performed for turbulent flow for the three-inlet mass flow 0.23lps,0.12lps and 0.06lps. The Reynolds number for all cases is between 8000 and 16,000.

The thermal governing equations of this heating system in a two dimensional configuration and unsteady state conditions, are given by the continuity equation, conservation of energy equation which discretized using the first order upwind scheme, conservation of momentum equation is discretized using the second order upwind scheme. The SIMPLE (Semi-Implicit Method for Pressure Linked Equations) algorithm was selected for Pressure–velocity coupling.

These equations for the fluid domain are given in a general Cartesian form as below. The differential equation describing the principle of conservation of mass which is valid for incompressible and compressible flows:

`

$$\frac{\partial \rho}{\partial t} + \frac{\partial}{\partial x_i}(\rho u_i) = 0 \quad (1)$$

Energy equation is given in Eq. (2)

$$. \frac{\partial}{\partial t}(\rho E) + \frac{\partial}{\partial x_i}[ui(\rho E + P)] = \frac{\partial}{\partial xj}(k_{eff}\frac{\partial T}{\partial x_i} + u_i(\tau_{ij})_{eff} + S_h \quad (2)$$

Where P is the static pressure, $(\tau ij)_{eff}$ is the stress tensor, the term $S_{h\ is}$ the defined the source term given by the equation:

$$S_h = \frac{-U_g \times A \times (T_S - T_a)}{V_r} \quad (3)$$

E is total energy represented by:

$$\text{E} = h - \frac{P}{\rho} + \frac{u_i^2}{2} \quad (4)$$

The stress tensor, $(\tau_{ij})_{eff})$ is given by the following correlation according:

$$\left(\tau_{ij}\right)_{eff}) = \mu_{eff}\left[\frac{\partial u_i}{\partial x_j} + \frac{\partial u_j}{\partial x_i}\right] - \frac{2}{3}\,\delta_{ij}\mu_{eff}\frac{\delta u_k}{\delta u_k} \quad (5)$$

where μ is the molecular viscosity, I is the unit tensor, and the second term on the right hand side is the effect of volume dilation.

The differential equation describing conservation of momentum for a Newtonian fluid flow is written:

$$\frac{\partial u}{\partial t} + u_i\,\frac{\partial u_i}{\partial x_i} = -\frac{1}{\rho}\frac{\partial P}{\partial x_i} + \frac{\partial}{\partial x_j}(\mu\frac{\partial u_i}{\partial x_j}) \quad (6)$$

To solve the governing equations numerically, the turbulence closure model used here is the standard K-ε to analyze turbulent properties of the flow. This model is introduced by Launder and Spalding (1974) and gives a general description of turbulence by means of two transport equations. The original impetus of this model in moderate to high complexity flows is to improve the mixing-length model and to find an alternative to algebraically prescribing turbulent length scales. This model is suitable only for fully turbulent flows.

The turbulence kinetic energy K equation is expressed in Eq. (7) (Ahsan, M.2014).

$$\frac{\partial}{\partial t}(\rho k) + \frac{\partial}{\partial x_i}(\rho k u_i) = \frac{\partial}{\partial x_j}[(\mu + \frac{\mu_t}{\sigma_k}\frac{\partial k}{\partial xj}] + G_k + G_b - \rho_\varepsilon - Y_m + S_k \quad (7)$$

The equation of the specific turbulent energy dissipation ε is expressed in Eq. (8)

`

$$\frac{\partial}{\partial t}(\rho\varepsilon) + \frac{\partial}{\partial x_i}(\rho\varepsilon u_i) = \frac{\partial}{\partial x_j}\left[\left(\mu + \frac{\mu_t}{\sigma_\varepsilon}\right)\frac{\partial \varepsilon}{\partial x_j}\right] + C1\varepsilon\frac{\varepsilon}{k}(G_k + G_{3\varepsilon}G_b) \qquad (8)$$

$$-G_{2\varepsilon}\rho\frac{\varepsilon^2}{k} + S_\varepsilon$$

where $G_k$, $G_b$, $Y_m$ in Eq. (7) represent the generation of turbulence kinetic energy due to the mean velocity gradients, is the generation of turbulence kinetic energy due to buoyancy and the contribution of the fluctuating dilatation in compressible turbulence to the overall dissipation rate, respectively. In addition, $C_{1\varepsilon}$, $G_{2\varepsilon}$ and $G_{3\varepsilon}$ are constants. The coefficients $\sigma_k$ and $\sigma_\varepsilon$ are the turbulent Prandtl numbers for k and ε, respectively. The $S_k$ and $S_\varepsilon$ are user-defined source terms. The constants of the model, are presented in Table 3.3.1.

Table 3.3.1 Constants values of the k-ε model.

| **Cμ** | **$C_{1\varepsilon}$** | **$C_{2\varepsilon}$** | **$C_{3\varepsilon}$** | **$б_k$** | **$б_\varepsilon$** |
|---|---|---|---|---|---|
| **0.09** | 1.44 | 1.92 | 1 | 1 | 1.3 |

The floor surface average temperature is calculated by Eq. (10)

$$T_S = \frac{1}{S}\int_0^S T_{i0}\ dx \qquad (9)$$

The homogenization level of heat distribution on the floor surface is extremely important. A new parameter for characterizing this level is represented by

$$Tm = \frac{1}{\sum_c A_c}(\sum_c A_c T_c) \qquad (10)$$

$$\sigma = [\frac{1}{\sum_c A_c}[\sum_c (A_c(T_c - T_m)^2)]^{1/2} \qquad (11)$$

where $A_c$ is the surface of element ($m^2$), $T_c$ is the cell temperature (°C) and $T_m$ is the mean temperature (°C).

The high values of σ indicate that there is a high heterogeneity of temperature at the floor surface.

`

### 3.3.2 Mesh Generation

The mesh generation for three different layout offset serpentine, counterflow and counter flow with different inlet position is shown in figure 3.3.2. Creating a high-quality mesh is one of the most critical factors that should be considered to ensure simulation accuracy. For this study tetrahedral meshing was generated which involves dividing the 3D geometry into tetrahedral elements. The default or automatic meshing was used to mesh the geometry. As the concrete and pipe is complex geometry, tetrahedral element meshing is considered to be the best choice. It is commonly used for complex and irregular geometries which can handle internal boundaries, such as fluid-solid interfaces, and capture fine details without requiring excessive refinement.

The mesh generation process plays a crucial role in accurately simulating the fluid flow behavior in various piping layouts. In the offset serpentine layout, as depicted in figure 3.3.2 (a), a fine mesh with 4.5 million tetrahedral elements and 980,450 nodes was generated. The default target skewness of 0.9 was set to ensure mesh quality. For the counterflow layout, shown in figure 3.3.2 (b), the meshing resulted in 4 million tetrahedral elements and 883,120 nodes. Likewise, for the counterflow layout with different inlet positions, as shown in figure 3.3.2 (c), the meshing process produced 4.3 million tetrahedral elements and 890,386 nodes. The meshing procedure is crucial to capture the intricate details of the fluid flow patterns and temperature distribution accurately. The generation of high-quality meshes allows for reliable and precise simulations, providing essential data for analyzing the thermal behavior and optimizing the designs of these piping layouts.

A linear mesh order has been applied along the surface and along the boundary region. The element size used for all three layout is 50mm.The size of elements was made as small as possible to capture every detail of the flow, thus, improving solution accuracy. The zone near the fluid domain has a much denser mesh to capture more data and get more accurate results.

.

`

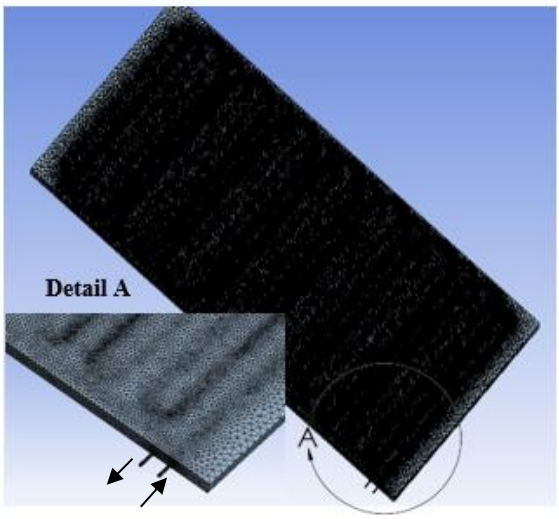


(a). Mesh generation for offset serpentine layout

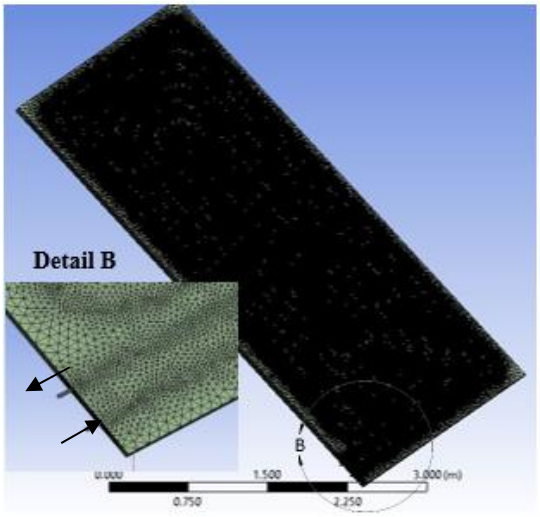


(b) Mesh generation for Counterflow layout

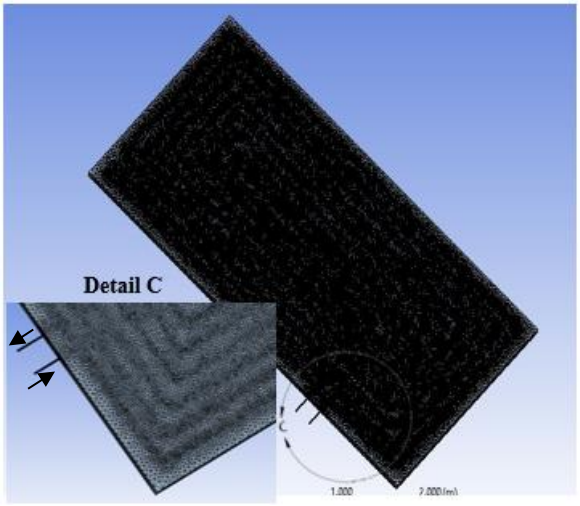


(c) Mesh generation for counterflow layout with different inlet position

Figure 3.3.2: Mesh Structure of concrete and pipe for three layouts

`

### 3.3.3 Boundary conditions

In order to simplify the numerical simulation model of the under-floor heating system, the theoretical heat transfer models are expressed by the following assumptions:

- Flow in the pipe is considered incompressible
- Steady-state condition assumption.
- Pipe thickness is considered negligible

The governing equations considered are the continuity equation, conservation of energy equation, and conservation of momentum equation. In this case, the domain of solution includes two different components; concrete block and the fluid system.

This study focused on the steady-state simulations for different piping layout embedded within the floor. The inlet has mass flow inlet and inlet temperature; the outlet has outflow condition. Coupled wall was used to define interaction between the fluid-flow domain and concrete**.** All the lateral walls of the configuration are assumed adiabatic. The boundary conditions are based on research done in Solar underfloor heating by S. K. Mishra, 2017.

The boundary conditions are presented below:

Table 3.3.3: Boundary Condition

| Layout | Location | Value |
|---|---|---|
| Offset serpentine / Counterflow | Inlet mass flow<br>Inlet temperature | 0.23 Lps<br>323k |
| | Outlet<br>Wall-fluid domain interface<br>Freestream temperature<br>Convection coefficient of air<br>Floor Bottom | Pressure outlet<br>Coupled<br>297k<br>10 $W/m^2k$<br>Insulated |

`

For this study the boundary condition, the floor dimension, pipe length, pipe spacing and overall floor construction design is taken from the research conducted by S. K Mishra, 2017. The model is recreated with modification in pipe layout.

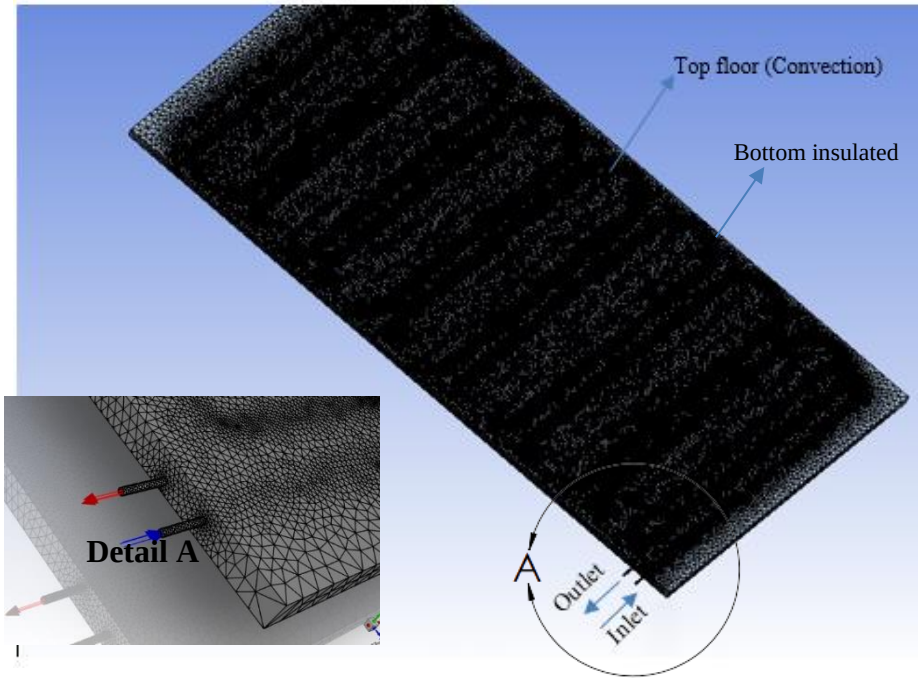


`

Figure 3.3.3: Boundary conditions for CFD simulation for offset serpentine layout

`

# CHAPTER FOUR: RESULT AND DISCUSSION

## 4.1 Temperature distribution for Offset Serpentine and Counterflow layout

### 4.1.1 Temperature distribution on floor surface for offset serpentine

The thermal analysis was done using ANSYS CFD and the temperature distribution on the floor surface was generated.

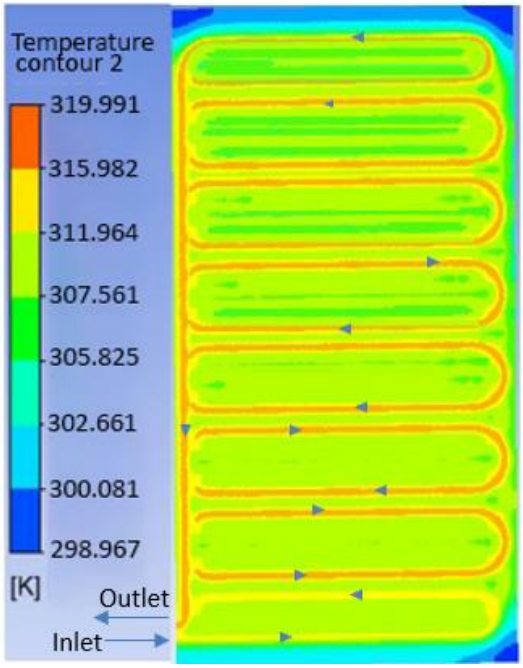


Figure 4.1.1: Temperature distribution for offset serpentine loop

The temperature distribution for Offset Serpentine layout is shown in figure 4.1.1. It is observed that a low-temperature region forms on the floor surface as the water flows towards the outlet. When the mass flow rate is 0.23 Lps, the overall floor temperature near the surface is around 307K. Temperature drops are seen near the bend region, particularly above the mid region of the floor. At the mid region, the temperature is around 305K, and it spreads to a larger area as the fluid passes to the top of the floor. As the water flows towards the outlet, the floor temperature drops by 2K near the top region, resulting in uneven temperature distribution on the floor surface. The temperature difference between the entry and exit of the loop is approximately 8K. This can be due to the multiple bends in the pipe circuit, creating a significant temperature gradient that affects the thermal comfort level. Some areas have slightly lower temperatures, possibly due to longer pipe lengths. Comparing this model to a study by S.K. Mishra in 2017, their serpentine layout had a temperature gradient of 5K, which is 3K less than what we observed. However, the overall floor temperature in this study is higher at 307K.

`

### 4.1.2 Temperature distribution for counterflow layout

The temperature distribution for the counterflow layout is shown in figure 4.1.2. When the bend radius is 190mm, the temperature is evenly distributed across the floor surface. In figure 4.1.2 (a), with a mass flow of 0.23 lps, the temperature near the bend drops by about 1.5K, while the overall floor surface temperature is approximately 309K. The temperature difference between the entry and exit of the loop is about 5K. When the mass flow is reduced to half (0.12lps), the overall floor temperature remains at 307K throughout the floor surface, and near the bend region, it drops to 305.36K. Cold spots start to form near the bend and become more prominent with reduced flow rates. As shown in figure (b), the low-temperature zone begins to form near the bend region, and it is smaller near the corners but grows larger as the fluid flows towards the center. In a study by S.K. Mishra in 2017, the counterflow layout had a temperature gradient of 1K, which is 4K less than what we observed. However, our counterflow layout shows an overall floor temperature of 309K for a mass flow of 0.23lps, which is higher than the analysis conducted by S.K. Mishra in 2017.

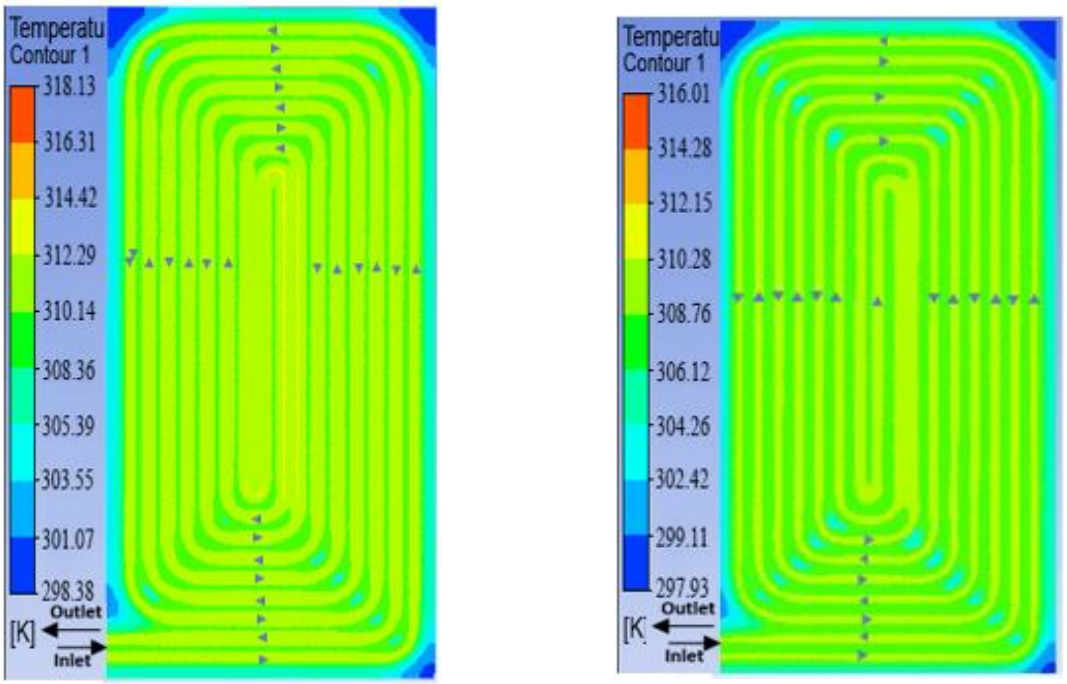


(a) Temperature distribution for mass flow 0.23Lps

(b) Temperature distribution for mass flow 0.12Lps

Figure 4.1.2 Temperature Distribution for Counterflow layout

`

## 4.2 Analyze the pressure gradient and turbulent kinetic energy for Offset serpentine and counterflow layout

### 4.2.1 Pressure Gradient for offset serpentine layout

The pressure gradient for the offset serpentine layout is illustrated in Figure 4.2.1. As the fluid flows towards the outlet in the offset serpentine layout, a significant pressure gradient near the bend region was observed. The maximum pressure gradient of 50,680 kg $m^{-2}s^{-2}$ was seen near the small bend, while it was much lower at 5010 kg $m^{-2}s^{-2}$ in the straight pipe section. The pressure gradient in the large bend section was measured at 20,154 kg $m^{-2}s^{-2}$, which was nearly half of that in the small bend section. The pressure gradient is higher near the small bend compared to the large bend section. The multiple bends in the offset serpentine layout create resistance to flow, resulting in increased pressure drop along the pipe. This can negatively affect the efficiency of fluid flow, and it might require more powerful pumps or increased energy consumption to maintain the desired flow rate.

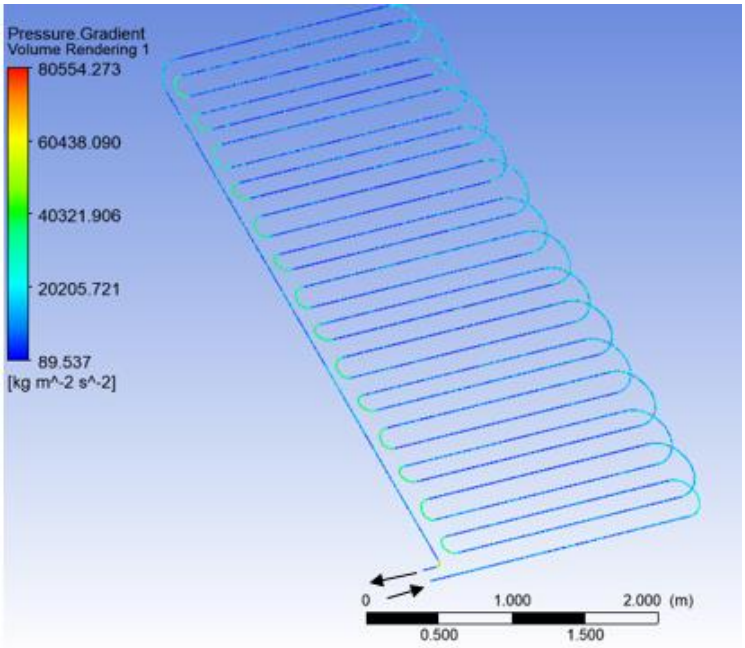


Figure 4.2.1 Pressure Gradient for offset serpentine layout

### 4.2.2 Pressure Gradient for counterflow layout

The pressure gradient for the counterflow layout is illustrated in Figure 4.2.2. This gradient represents the change in pressure along a specific direction. As the fluid flows towards the outlet, the maximum pressure gradient was observed near the bend, while it was lower in the straight pipe section. The larger bend section located on the floor corners

`

showed a minimal pressure drop compared to the smaller bend region towards the center region. Specifically, for the counterflow layout, a maximum pressure gradient of 25,070 $kgm^{-2}s^{-2}$ was observed near the smaller bend in the central region, while the minimum gradient of 1,500 $kgm^{-2}s^{-2}$ was observed in the straight pipe section. In Detail A view of the figure, the pressure gradient at the bend section near the center region was 18,164 $kgm^{-2}s^{-2}$, whereas at the corner bend, it was only 15,100 $kgm^{-2}s^{-2}$. The pressure gradient in the bend region is higher than that in the straight pipe, resulting in higher pressure loss. Understanding these pressure gradients is crucial for optimizing the layout's efficiency and minimizing pressure-related issues in the piping system.

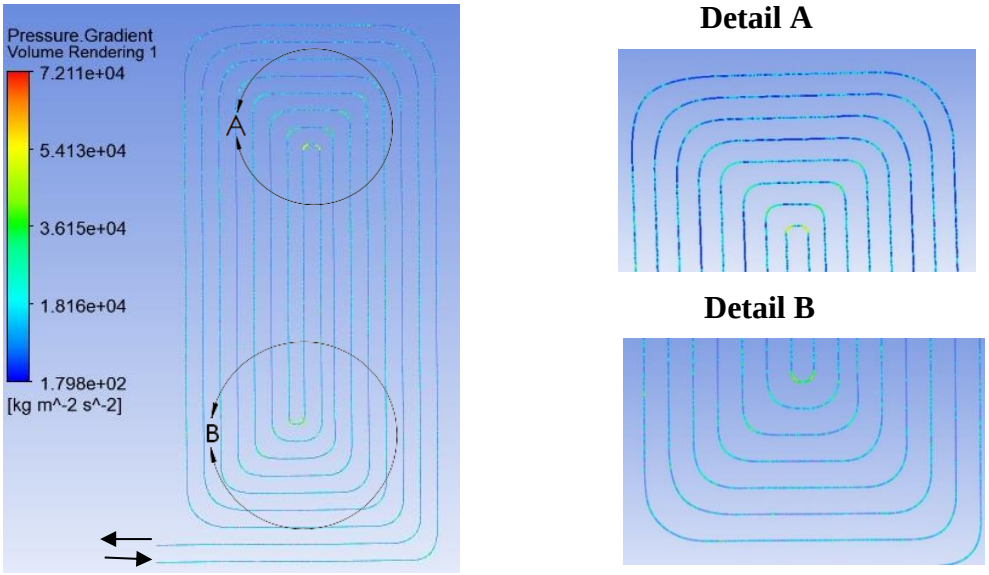


Figure 4.2.2 Pressure Gradient for Counterflow layout

### 4.2.3 Turbulent Kinetic Energy for offset serpentine

The turbulent kinetic energy for the offset serpentine layout is depicted in figure 4.2.3. This measurement indicates the intensity of turbulence in the flow. In fluid system design, turbulence is crucial for heat or mass transfer. As the fluid flows towards the outlet, more turbulence was observed near the small bends than in the large bend region. The turbulence levels in the small bend region and large bend section were $0.327m^2s^{-2}$ and $0.18m^2s^{-2}$ respectively. This means that the turbulence in the small bend region was twice as much as in the large bend section. In contrast, the flow was less turbulent in the straight pipe region. This uneven flow distribution affects thermal comfort. The turbulent flow starts to form as the flow passes near the bend region, and it decreases as it flows through the straight pipe section. Understanding and controlling turbulence in the piping system are essential for optimizing heat and mass transfer processes.

`

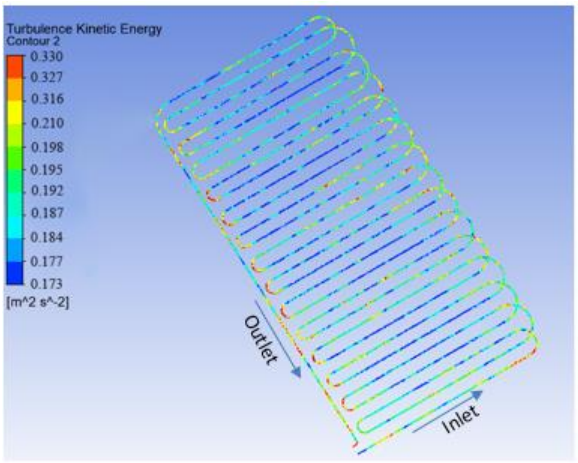


Figure 4.2.3 Turbulent Kinetic Energy Serpentine Layout

### 4.2.4 Turbulent Kinetic Energy for counterflow layout

The turbulent kinetic energy (TKE) for the counterflow layout is shown in figure 4.2.4. As the fluid flows towards the outlet, higher turbulence was observed near the bend region. The turbulence level near the bend region was measured at 0.0703 $m^2s^{-2}$, while in the straight pipe region, it was 0.0287 $m^2s^{-2}$. As the flow passes near the bend region, the turbulent flow starts to form, and it decreases as it moves through the straight pipe section. The flow in the straight pipe region is less turbulent. Typically, TKE in a bend pipe is higher compared to straight pipe flows due to additional mixing and shearing effects induced by the curvature. This uneven flow distribution affects thermal comfort. Understanding and managing TKE levels are essential to ensure a stable and predictable flow within the pipe, reducing the risk of flow-induced issues. Controlling turbulence helps to optimize flow patterns and ensures efficient heat or mass transfer in the counterflow layout.

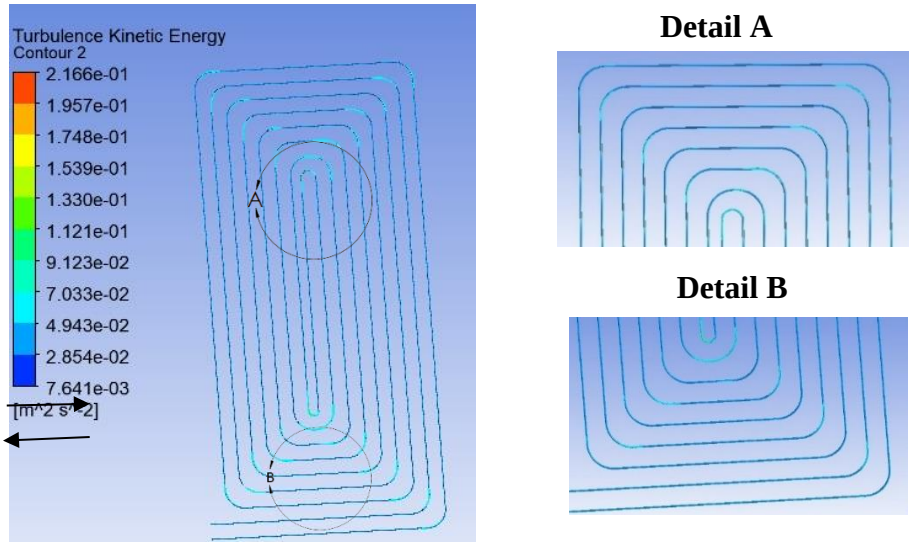


Figure 4.2.4 Turbulent kinetic Energy Counterflow Layout

`

### 4.3 Analyze the temperature distribution near the bend for counterflow layout with bend radii 2mm,20mm,30mm,40mm,50mm,65mm and 190mm

The counterflow layout as shown in Figure 4.1.2 indicated that there was a temperature drop near the bend region for bend radius 190mm. So, the radius of bend for counterflow layout was varied to 2mm, 20mm,30mm,40mm,50mm,65mm and temperature distribution for different mass flow was observed.

#### 4.3.1 Case 1: Bend Radius 2mm

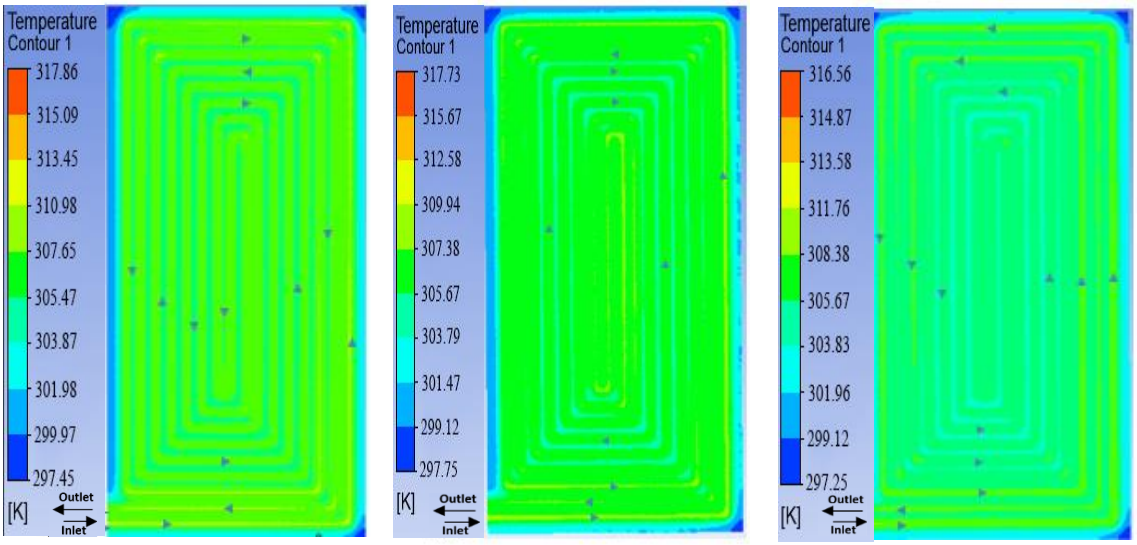


(a) 0.23 lps massflow (b) 0.12 Lps mass flow (c)0.06 lps massflow

Figure 4.3.1 Temperature distribution for 3 different mass flow with bend radius 2mm

The temperature distribution for the counterflow layout with a bend radius of 2mm is shown in figure 4.3.1. For a mass flow of 0.23 Lps, a slight drop in temperature between the pipes towards the center region was observed, while the temperature remained uniform near the floor corners. The temperature between the pipe spacing was 306K near the center region and 307K near the floor corner. As the mass flow was reduced to half (0.12Lps), the temperature between the pipe spacing further dropped to 304K, but it remained uniform near the edges. The temperature near the center region further dropped to 303K as the mass flow was reduced to 0.06Lps. With reduced mass flow, the temperature near the floor edges also decreased. When water flows through sharp bends, it creates resistance, leading to uneven flow rates and temperature variations in the floor.

`

### 4.3.2 Case 2: Bend Radius 20mm

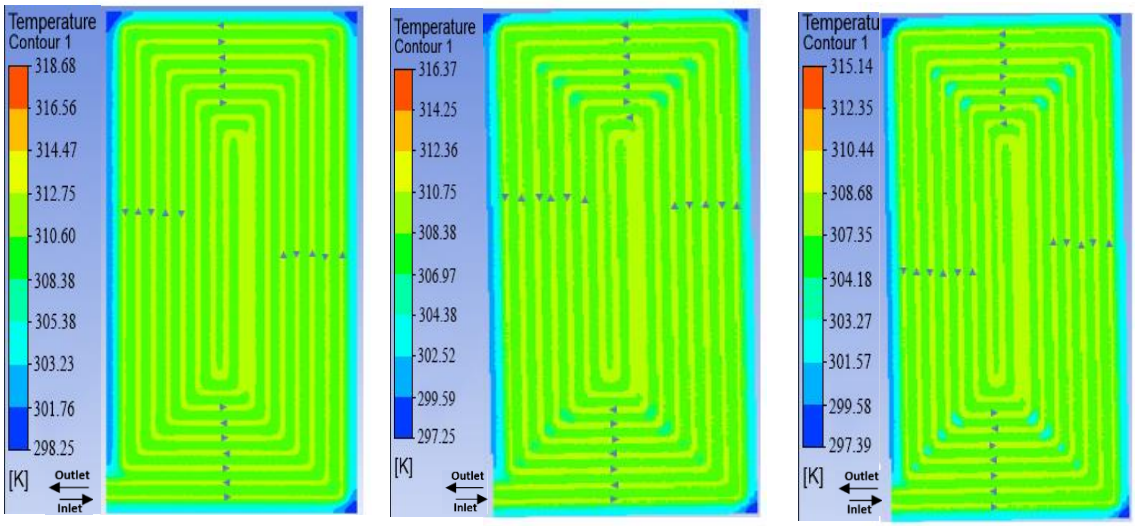


(a)0.23 lps massflow (b) 0.12 lps massflow (c)0.06 lps massflow

Figure 4.3.2 Temperature distribution for 3 different mass flow for bend radius 20mm

The temperature distribution for the counterflow layout with a bend radius of 20mm is illustrated in figure 4.3.2. At a mass flow rate of 0.23Lps, the temperature on the floor surface was uniform, with an overall floor temperature of 309K and 308.4K near the bend. There was no significant temperature drop on the floor surface, but a temperature drop was observed near the floor corner, where the floor wall had a temperature of 304K. When the mass flow was reduced to half (0.12Lps), the temperature remained even throughout at 307K, except in the corner region where a few low-temperature regions were created near the bends in the center. At a mass flow rate of 0.12Lps, the temperature near the bend was 306.25K. Further reducing the mass flow to 0.06Lps resulted in an overall floor temperature of 305K, while the temperature near the bend dropped to 304K and continued to grow towards the center region. As the mass flow was reduced, the temperature started to drop near the center and continued to grow towards the corner bend.

### 4.3.3 Case 3: Bend Radius 30mm

The temperature distribution for the counterflow layout with a bend radius of 30mm is presented in figure 4.3.3. At a mass flow rate of 0.23lps, the temperature on the floor surface was uniform throughout, with an overall floor temperature of 309K and 308.87K near the bend.

`

There was no significant temperature drop on the floor surface, but a temperature drop was observed near the floor wall. When the mass flow was reduced to half (0.12Lps), the temperature remained even at 307K throughout, except in the corner region. At a mass flow rate of 0.12lps, a few low-temperature regions were created near the bend in the central region, and the temperature near the bend was 306.56K, while the overall floor temperature was 307K. Further reducing the mass flow to 0.06lps resulted in an overall floor temperature of 305.2K, while the temperature near the bend dropped to 304.5K and continued to grow towards the center region.

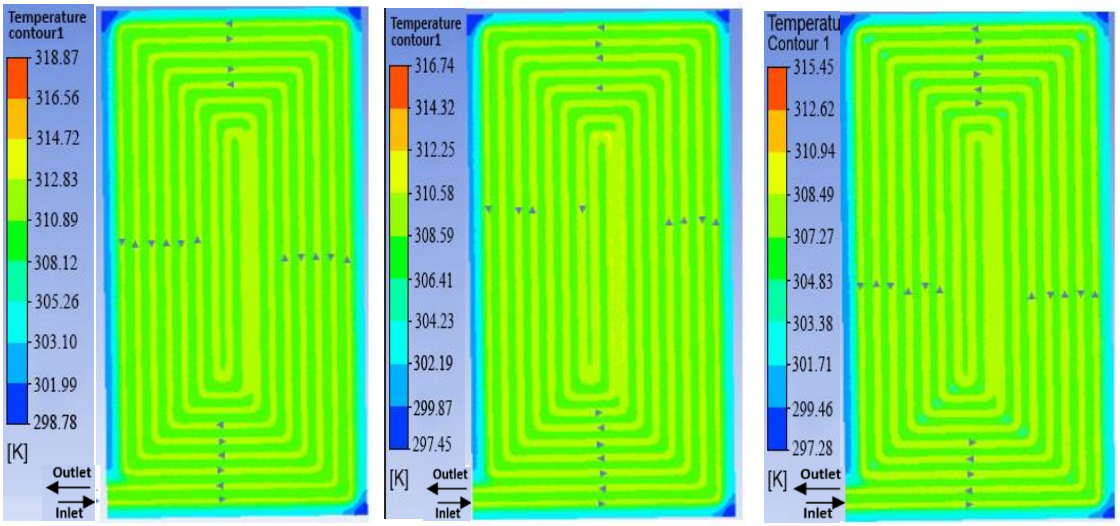


(a)0.23 Lps mass flow (b)0.12 Lps mass flow (c) 0.06 Lps mass flow

Figure 4.3.3 Temperature distribution for 3 different mass flow for bend radius 30mm

### 4.3.4 Case 4: Bend Radius 40mm

The temperature distribution for the counterflow layout with a bend radius of 40mm is depicted in figure 4.3.4. At a mass flow rate of 0.23 Lps, the temperature on the floor surface was uniform throughout, with an overall floor temperature of 309K and 308.53K near the bend. There was no significant temperature drop observed on the floor surface and near the bend. When the mass flow was reduced to half (0.12Lps), the temperature remained even throughout, except in the corner region. A few low-temperature regions were created near the bends in the central region. At a mass flow rate of 0.12Lps, the temperature near the bend was 306.47K. Further reducing the mass flow to 0.06Lps resulted in an overall floor temperature of 305K, while the temperature near the bend dropped to 304.2K and continued to grow across all bend regions and towards the center region

`

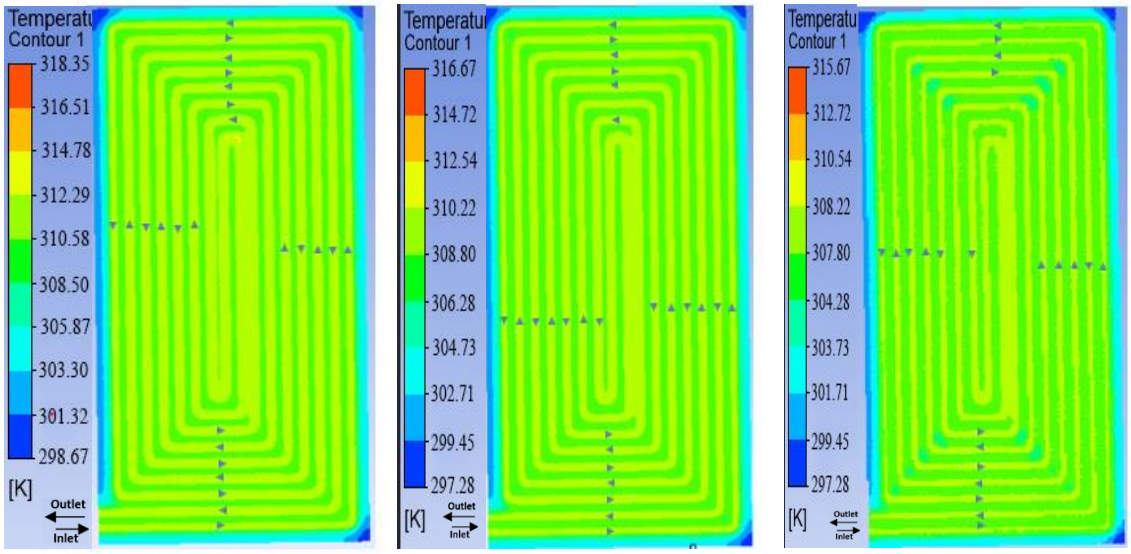


(a) 0.23 Lps mass flow (b) 0.12 Lps mass flow (c) 0.06 Lps mass flow

Figure 4.3.4 Temperature distribution for 3 different mass flow for bend radius 40mm

### 4.3.5 Case 5: Bend Radius 50mm

The temperature distribution for the counterflow layout with a bend radius of 50mm is shown in figure 4.3.5. At a mass flow rate of 0.23Lps, the overall floor temperature was 309K, and it was 308.02K near all the bend sections. The temperature drop started to form near the bend region, and a few low-temperature zones of small size were formed near all bends. There was no significant temperature drop observed on the floor surface. When the mass flow was reduced to half (0.12Lps), the temperature remained even throughout the floor surface, except in the corner and bend regions. The low-temperature region increased in size near the bends as the flow was reduced to half. A few low-temperature regions were created near all bend regions, with temperatures of 306.1K. Further reducing the mass flow to 0.06Lps resulted in the temperature near the bend dropping to 303.8K and continuing to grow across all bend regions.

`

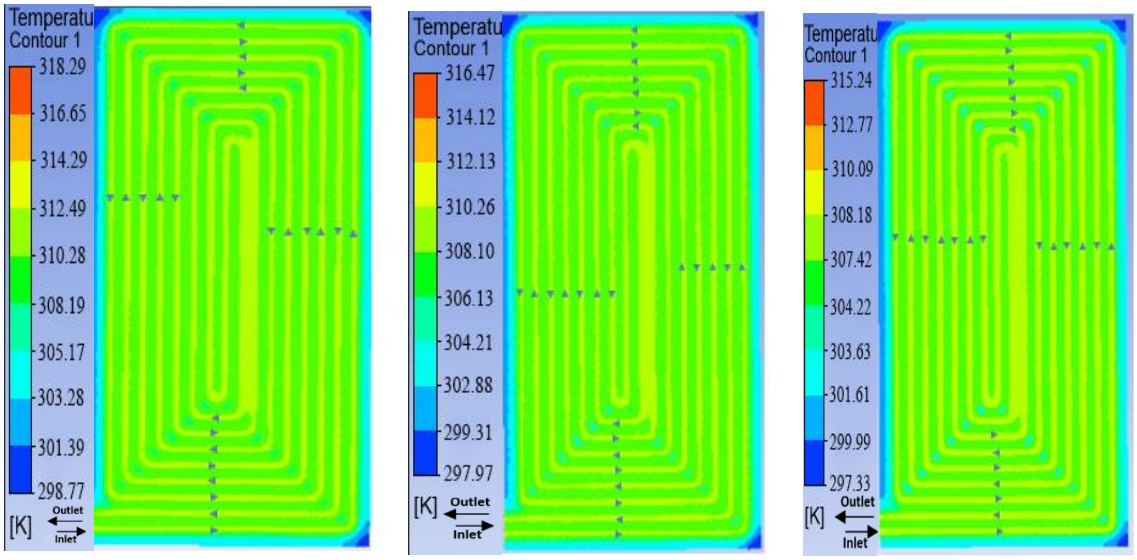


(a) 0.23 Lps mass flow (b) 0.12 Lps mass flow (c) 0.06 Lps mass flow

Figure 4.3.5 Temperature distribution for 3 different mass flow for bend radius 50mm

### 4.3.6 Case 6: Bend Radius 65mm

The temperature distribution for the counterflow layout with a bend radius of 65mm is presented in figure 4.3.6. At a mass flow rate of 0.23Lps, the overall floor temperature was 309K, while it was 307.87K near the bend in the central region. A temperature drop near the bend in the central region was observed, while there was no temperature drop near the bend in the corner region. When the mass flow was reduced to half (0.12Lps), the temperature remained even throughout the floor surface at 307K, except in the corner and bend regions. A low-temperature region was created near all bends, and the temperature drop was 305.87K. Further reducing the mass flow to 0.06Lps resulted in an overall floor temperature of 304K, while the temperature near the bend dropped to 303.57K and continued to grow its shape across all bend regions. The maximum low-temperature region was in the central region near the bend, and it spread larger as the mass flow was reduced.

`

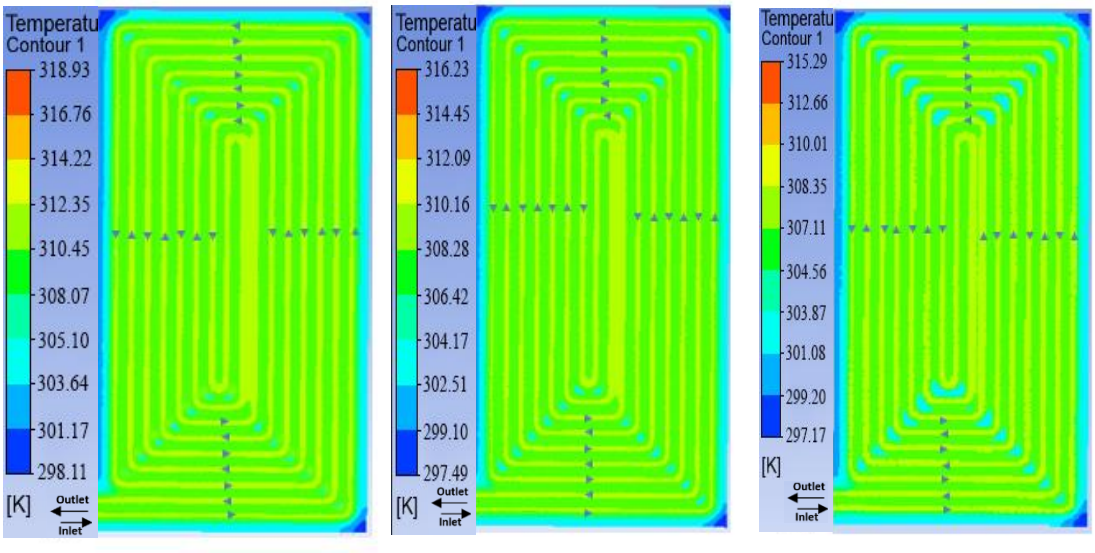


(a) 0.23 Lps mass flow (c) 0.12 Lps mass flow (b) 0.06 lps mass flow

Figure 4.3.6 Temperature distribution for 3 different mass flow for bend radius 65mm

### 4.3.7 Case 7: Bend Radius 190mm

The temperature distribution for the counterflow layout with a bend radius of 190mm is shown in figure 4.3.7. At a mass flow rate of 0.23Lps, the overall floor temperature was 309K, while it was 307.54K near the bend. A temperature drop near the bend in the corner region was observed. When the mass flow was reduced to half (0.12Lps), the temperature remained even throughout the floor surface at 307K, except in the corner and bend regions. The temperature near the bend was 305.36K. The low-temperature region started to form near the bend and grew all over the bend region as the mass flow rate was reduced. Further reducing the mass flow to 0.06Lps resulted in an overall floor temperature of 305K, while the temperature near the bend dropped to 303.13K and continued to grow its shape across all bend regions. The floor corners experienced a sharp decrease in temperature as the mass flow rate was reduced. The low-temperature region near the bend was larger and more significant in the center region than the corner region.

`

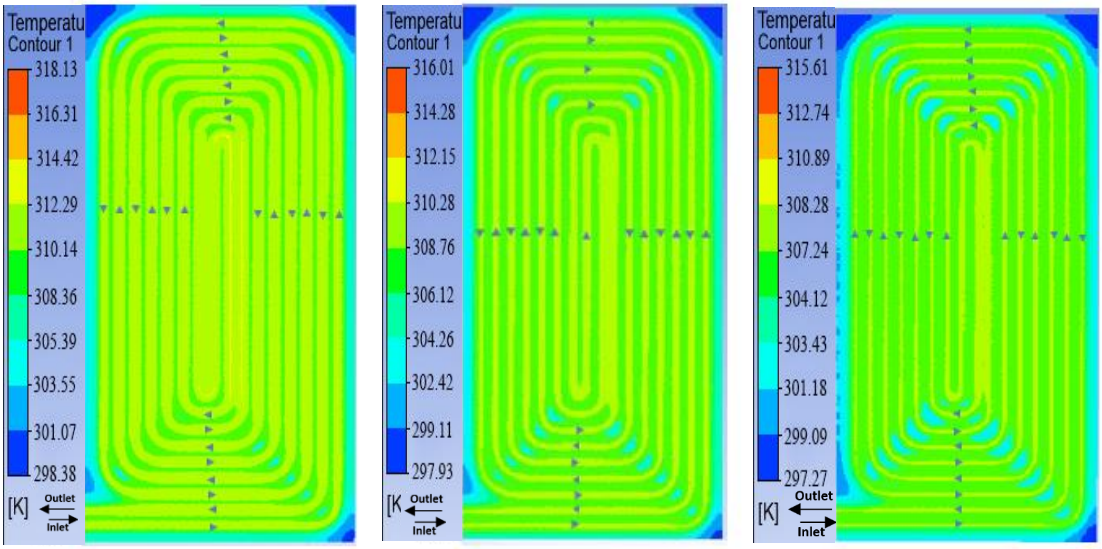


(b) 0.23 Lps massflow (a) 0.12 Lps massflow (b) 0.06 Lps massflow

Figure 4.3.7 Temperature distribution for 3 different mass flow for bend radius 190mm

### 4.3.8 Summary of Temperature near bend for various bend radii

The graph below presents the temperature variations near the bend for a counterflow layout with different bend radii (2mm, 20mm, 30mm, 40mm, 50mm, 65mm, 190mm) and three distinct mass flow rates (0.23lps, 0.12lps, and 0.06lps). Analyzing the chart reveals the significant influence of inlet mass flow rate and bend radius on the temperature distribution along the bend. It is seen that the temperature near the bend region is affected by the bend radius. For a constant pipe spacing as the bend radius is increased the temperature starts to drops gradually near the bend. As seen on graph, for a mass flow of 0.23Lps and bend radius 2mm the bend temperature was 306K. As the bend radius increases to 30mm, the temperature near the bend reaches its peak and subsequently starts to decrease slightly. Beyond a bend radius of 40mm, it becomes evident that the temperature near the bend region gradually decreases for all three mass flow rates. When examining the effect of mass flow rates, it was observed that a larger mass flow rate (0.23lps) led to a smaller temperature drop of approximately 0.2K with changes in bend radius. In contrast, a sudden drop-in mass flow rate (0.06lps) resulted in a more significant temperature drop of over 0.4K. The temperature drop near the bend was larger for large bend with decrease in mass flow rate.

`

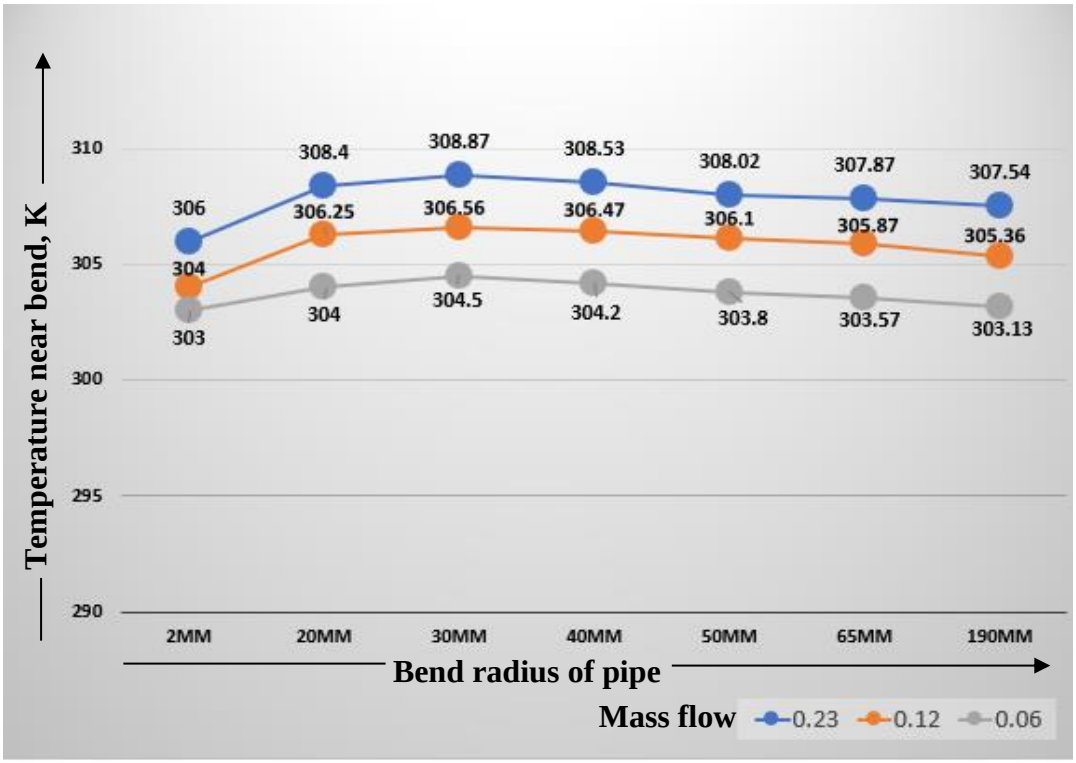


Figure 4.3.8 Temperature near bend for various bend radii and mass flow rate

## 4.4 Analyze the effect of inlet pipe position on temperature distribution for counterflow layout for different mass flow rate

### 4.4.1 Case B: Temperature distribution for counterflow layout with a different inlet position

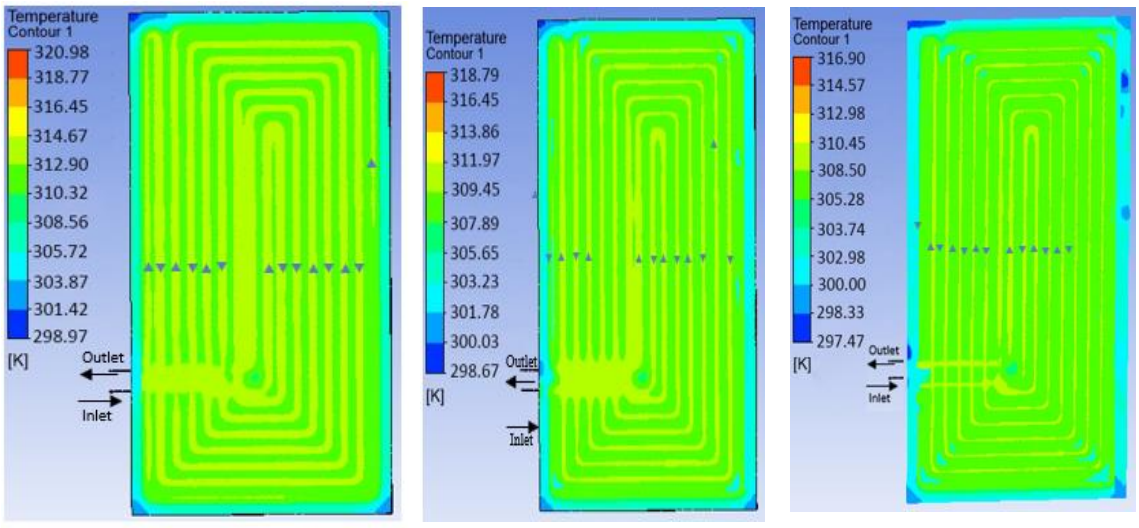


(a) 0.23 Lps mass flow (b) 0.12 Lps massflow (c) 0.06 Lps mass flow

Figure 4.4.1 Temperature distribution for counterflow with change in inlet pipe position

`

The temperature distribution on the floor surface for the counterflow layout with a change in inlet position is shown in figure 4.4.1. The analysis is conducted for 3 different mass flow rates: 0.23lps, 0.12lps, and 0.06lps, respectively. At a mass flow rate of 0.23lps (as shown in figure 4.4.1 (a), the overall temperature distribution throughout the floor surface was uniform at 310K. The floor corners formed a low-temperature region of 305K, and no temperature drop was observed near the bend region. The temperature on the floor surface near the wall region was about 309K. The outlet temperature for this piping layout is 320K, and there is a difference of 3K between the entry and outlet temperatures.

As shown in figure 4.4.1 (b) the mass flow rate was reduced to half 0.12lps and the temperature distribution on the floor surface was observed. The overall floor surface temperature was 308K, and the wall corners developed a low-temperature region. Additionally, it was noticed that a few bend regions near the corners had a low-temperature zone of 305K. The reduced mass flow resulted in the growth of a low-temperature zone near the floor walls and also near the outlet region. As the fluid circulated from the center to outwards, the central region had no temperature drop, while the pipe corner bend developed a low-temperature region.

As shown in figure 4.4.1 (c) the mass flow rate was further reduced to 0.06 lps and the temperature distribution on the floor surface was observed. The overall floor surface temperature was 305K, and the outlet temperature was 316K. As we reduced the mass flow rate, we observed the formation of a few low-temperature regions of 302K near the bend region on the floor corners. The temperature near the floor walls grew larger in size, and a temperature drop of 302K near the inlet and outlet regions was noticed. However, no temperature drop was observed near the bend in the central region. The reduction in mass flow rate resulted in a few cold spots of 297K near the floor wall.

### 4.4.2 Comparison of Counterflow layout Case 3 and Case B

The piping layout for both Case 3 and Case B was simulated with three different mass flows, and the obtained results were compared. In Case 3, the adjacent loops of the piping system have opposite directions of water flow, with the fluid moving from the floor corner towards the center. On the other hand, Case B exhibits a fluid flow scenario from the center to outward. Both Case 3 and Case B have same bend radius of 30mm.

The temperature distribution across the floor surface was compared between Case 3 and Case B. Case B exhibited a slightly higher overall temperature, with a difference of 1k

`

compared to Case 3. When both layouts had a mass flow of 0.23lps, they both experienced a temperature drop near the floor walls. However, as the mass flow was reduced, a noticeable difference was seen. In both cases, few low-temperature zones began to form near the bends. For Case 3, the temperature drop initiated near the bend in the center region, while for Case B, the low-temperature zone emerged near the wall corner bends.

As the mass flow rate was reduced, distinct differences in temperature distribution were observed between Case 3 and Case B. In Case 3, the size of the temperature drop region near the floor wall was smaller compared to Case B, where the drop was larger. Specifically, at a mass flow rate of 0.12lps, Case 3 exhibited a temperature of 306.76K near the bend, with an overall floor temperature of 307K. However, in Case B, the overall floor surface temperature increased to 308K, and low-temperature regions developed at the wall corners. Furthermore, in Case B, bend regions near the corners experienced a low-temperature zone of 306K.

Upon reducing the mass flow to 0.06lps, temperature changes were observed for Case B and Case 3. In Case B, a few low-temperature regions of 302K formed near the bend on the floor corners, while the temperature near the floor walls increased in size, and a temperature drop of 302K was evident near the inlet and outlet region. However, no temperature drop was observed near the bend in the central region. Additionally, the reduction in mass flow rate resulted in a few cold spots of 297K near the floor wall. As for Case 3, further decreasing the mass flow to 0.06lps led to the temperature near the bend dropping to 303.7K and continuing to grow towards the center region.

`

# CHAPTER FIVE: CONCLUSION AND RECOMMENDATIONS

## 5.1 Conclusion

In this study, the temperature distribution in a concrete floor with a thickness of 75mm and a thermal conductivity of 0.8W/Km$^2$ was examined. The floor was equipped with 13mm diameter pipes, and the inlet temperature supplied was 323K. The temperature distribution for three layout offset serpentine, counterflow layout and counter flow layout with different inlet position was studied by varying the pipe bend radius for different mass flow rate.

The offset serpentine layout exhibited a larger temperature drop on the floor surface compared to the counterflow layout. The temperature at the outlet for the counterflow model was approximately 3K higher than that of the offset serpentine layout. For offset serpentine layout temperatures dropped noticeably near the bend region above the mid-region, resulting in some minor temperature variations across the floor. On the other hand, the counterflow layout exhibited a more uniform temperature distribution across the entire floor surface, showing consistent heat transfer characteristics. The comparison of pressure gradients and turbulence levels between the two layouts revealed that the offset serpentine layout exhibited higher values compared to the counterflow layout

The study observed the temperature variations near bends in a hydronic heating system with different pipe bend radii (ranging from 2mm to 190mm) and various mass flow rates. For the 2mm bend radius at low mass flow rates, it was found that reducing the pipe spacing towards the center can help achieve a more uniform temperature distribution. As the bend radius increased, the temperature near the bend initially rose until reaching 30mm, after which it started to decrease slightly. Furthermore, for bend radii beyond 40mm, the temperature near the bend showed a gradual decrease for all three tested mass flow rates. Overall, the study revealed that larger bend radii contributed to more substantial temperature drops near the bends, particularly when combined with decreased mass flow rates. To achieve optimal performance and uniform heat distribution, the most suitable and recommended bend radius for the FHS installation is within the range of 30mm to 40mm.

In this study, the impact of changing the inlet position for a counterflow layout in a Floor Heating System was investigated. The fluid flow was reversed, circulating from the floor center to the outer edges. This change in inlet position resulted in the fluid being preheated to some extent before reaching the central region. As a result, at a mass flow rate of

`

0.23lps, the temperature at the outlet was slightly higher, reaching 320K, and the overall temperature on the floor surface reached 310K. The findings suggest that the counterflow layout with the fluid circulating from the center to the outward direction is best suited for FHS installation. This layout allows for better preheating of the fluid, leading to a more even temperature distribution across the floor. Implementing this layout in FHS installations can significantly improve system efficiency and enhance the overall heating experience for occupants.

### 5.2 Recommendations

Providing optimal thermal comfort has become a priority in various residential, commercial, and industrial sectors, driving the need for advanced and efficient heating technologies. As people's expectations for comfortable indoor environments rise, there is an increasing sense of urgency to implement heating solutions that can meet these demands. Underfloor heating is an excellent heating solution that provides comfort, energy efficiency, and numerous benefits for residential and commercial spaces. Its ability to offer even heat distribution, flexibility in design, and health advantages makes it a compelling choice for modern building heating systems. As technology advances and sustainable heating solutions become more crucial, the research areas below can significantly contribute to the continuous improvement of hydronic radiant floor heating systems, making them even more attractive for energy-efficient and comfortable space heating applications.

- Experimental setup can be built for the same conditions and temperature at different layout can be measured for the validation of simulation results.
- The integration of hydronic radiant floor heating systems with renewable energy sources like solar thermal collectors, geothermal heat pumps, or waste heat recovery systems can be explored.
- Simulation of temperature distribution at the room for radiant heating system can be done using different approach for thermal comfort assessment.

`

## REFERENCES


Ahsan, M. (2014). Numerical analysis of friction factor for a fully developed turbulent flow using k-ε turbulence model with enhanced wall treatment. *Journal of Basic and Applied Sciences, 3*, 269-277.

ANSI/ASHRAE Standard 55-2017. Thermal Environmental Conditions for Human Occupancy.

Arefeh Hesaraki (2016). Integrating Low-temperature Heating Systems into Energy Efficient Buildings,3043 – 3048

ASHRAE, 2009 ASHRAE Handbook, SI Edition. USA: ASHRAE, 2009.

Banerjee, P. K., & Palmer, M. R. (1991). Experimental study of a radiant floor heating system. *Solar Energy, 47(2*), 111-119.

Borong Lin, Zhe Wang, Hongli Sun, Yingxin Zhu, Qin Ouyang (2016), Evaluation and comparison of thermal comfort of convective and radiant heating terminals in office buildings Build. Environ., 91-102 Central Heating (2017), Australia, Underfloor-Heating-Installation-Method,3-4

Damasceno F A, Oliveira C E A, Saraz J A O, Schiassi L & de Oliveira J L,2018 Validation of a Heating System in the Farrowing House using a CFD Approach, Engineering Agrícola,471–477

De Dear, R. J., Brager, G. S., Cooper, D., & Lee, Y. S. (2018). Developing an adaptive model of thermal comfort and preference. *ASHRAE Transactions*, 124(1), 56-70.

Eickhoff, W. R. (1962). Heat distribution in radiant panel floors. Transactions of the American Society of Heating, *Refrigerating and Air-Conditioning Engineers*, 68, 132-143.

Feng, J.S. Schiavon et al. (2013). Cooling load differences between radiant and air heating systems. *Energy and building* ,44-52

Gao, J., Chen, H., & Xiong, S. (2017). A review of HVAC technologies for energy efficient buildings. *Applied Energy*, 204, 1161-1174.

H. Khorasanizadeh G.A. et al. (2014). Numerical study of air flow and heat transfer in a two-dimensional enclosure with floor heating. *Energy and Buildings.62-70*

`

Hans-Martin Henning (2012). Solar systems for heating and cooling of buildings. *Energy Procedia* 633-653.

Haruo Hanibuchi (1998). Basic study of radiative and convective heat exchange in a room with floor heating. *ASHRAE Transactions*, 55-62

Hasan Karabay, MuslumArıcı, Murat Sandıkm A numerical investigation of fluid flow and heat transfer inside a room for floor heating and wall heating systems. *Energy Build*., 67 (2013), 471-478

Heba Al Maleh et al. (2011). Studying, Testing and simulating floor heating solar system. *Energy Procedia,* 337–346.

Hu R., J.L. Niu et al. (2015). A review of the application of radiant cooling and heating system in Mainland China. *Energy and Building*, 11-19

Humphreys, M. A., & Nicol, J. F. (2004). Understanding the adaptive approach to thermal comfort. *ASHRAE Journal*, 46(6), 24-28

IN-FLOOR RESIDENTIAL DESIGN & INSTALLATION GUIDE, 2022 Colorado: INFLOOR Heating Systems

Khorasanizadeh H, Sheikhzadeh G A, Azemati A A & Hadavand B S, (2014) Numerical study of air flow and heat transfer in a two-dimensional enclosure with floor heating, *Energy and Buildings*, 98–104

L. Yang, H. Yan, and J. C. Lam, "Thermal comfort and building energy consumption implications – A review," *Applied Energy*, vol. 115, pp

Launder, B. E., & Spalding, D. B. (1974). The numerical computation of turbulent flows. Computational Methods and Applied Mechanics Engineering, 3(2), 269-289.

Liu, R. (1979). Heat transfer in hydronic radiant panel systems. Transactions of the American Society of Heating, Refrigerating and Air-Conditioning Engineers, 85, 79-91.

Liu, T., & Li, B. (2015). Performance Comparison of Serpentine and Counterflow Layouts for Underfloor Heating Systems Using CFD Simulations. Energy and Buildings, 85, 465-471. DOI: 10.1016/j.enbuild.2014.10.058.

Malla, Sunil (2022), An outlook of end-use energy demand based on a clean energy and technology transformation of the household sector in Nepal, Volume 238, Part B

`

Man Sudhir (2017). Energy Efficient Building for Nepalese Market. Norway: Faculty of Engineering and Technology

Merabtine A., Kheiri A., Mokraoui S., Belmerabet A., (2019) Semi-analytical model for thermal response of anhydrite radiant slab. Building and Environment ,253-266.

Mi.Su Shin, KyuNam Rhee, Seong RyongRyu, Myoung Souk Yeo, Kwang Woo Kim, 2015 Design of radiant floor heating panel in view of floor surface temperatures. *Building Environment*, 559-577

Mishra S.K, "Design and Analysis of Solar Under Floor Heating System," *Tribhuvan University, IOE*, 2017.

Mohammad Javad Izadi and Kamyar Makaremi (2009). CFD simulation of temperature distribution in a room with various under floor heating system models. *In Proceedings of the ASME 2009 Fluids Engineering Division Summer Meeting*

Ngo, CC, Alhabeeb, BA, & Balestrieri, M. "Experimental Study on Radiant Floor Heating System." *Proceedings of the ASME 2015 International Mechanical Engineering Congress and Exposition*. Volume 8A: Heat Transfer and Thermal Engineering

Olesen & B.W (2012). Using building mass to heat and cooling. ASHRAE Journal,44-52

Ran Gao, Angui Li, Ou Zhang, Hua Zhang(2010) Comparison of indoor air temperatures of different under-floor heating pipe layouts. *Energy Conversion*.1295-1304

Sevilgen, G. Ö., & Kilic, M. (2011). Numerical analysis of air flow, heat transfer, moisture transport and thermal comfort in a room heated by two-panel radiators. Energy and Buildings, 43, 137-146.

Wang Y, Zhang X, Ji J, Tian Z, & Li Y, (2018) Numerical simulation of thermal performance of indoor airflow in heating room, *Proceedings of 10th International Conference on Applied Energy (ICAE2018)*, Hong Kong, China, 22-25

Wang Z, (2014). A review on radiant cooling system in building of china . *Energy and Building* ,101-108

Xiaozhou Wu, Yujia Liu, Genglin Liu. (2017). Effect of Supply Air Temperature on Indoor Thermal Comfort in a Room with Radiant Heating and Mechanical Ventilation. *Energy Procedia*, 206-213

`

Xiaozhou Wu, Jianing Zhao, Bjarne W. Olesen, Lei Fang, Fenghao Wang, (2015) A new simplified model to calculate surface temperature and heat transfer of radiant floor heating and cooling systems.,106-109

Xing Jin, Xiaosong Zhang, Yajun Luo, (2010 A calculation method for the floor surface temperature in radiant floor system, *Energy Buildings*.,1753-1758

Xing Jin, Xiaosong Zhang, Yajun Luo, Rongquan Cao, (2010), Numerical simulation of radiant floor cooling system: the effects of thermal resistance of pipe and water velocity on the performance. *Building Environment*., 2545-2552

Zheng X., Han Y., Zhang H., Zheng W., Kong D.,2107 Numerical study on impact of non-heating surface temperature on the heat output of radiant floor heating system. *Energy and Buildings* 198-206.

`

# APPENDIX A: Geometry Development

## Step 1: Geometry Development in Solid works

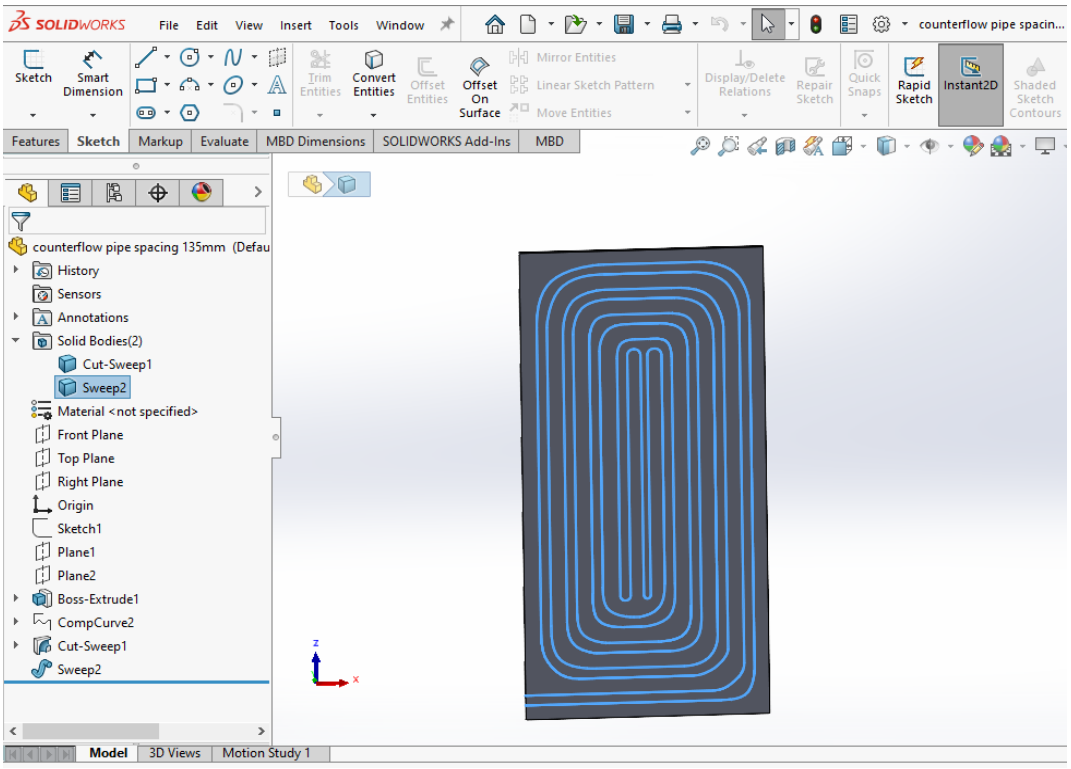


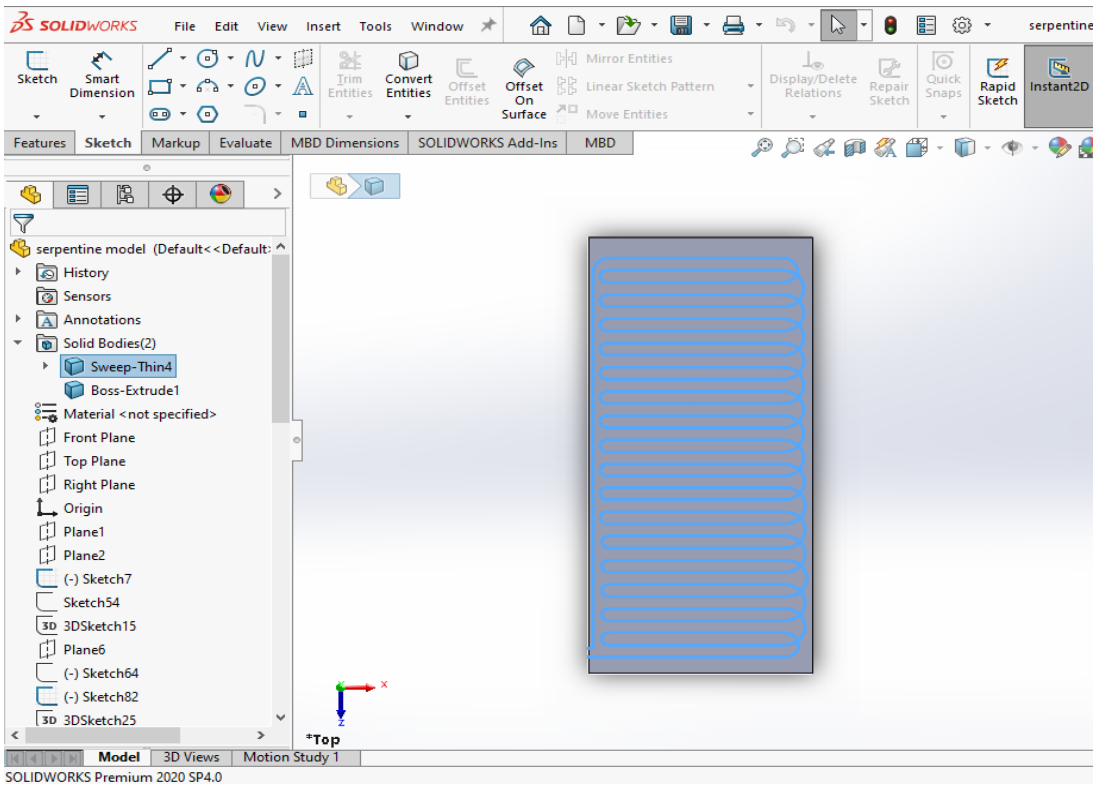

`

## Step 2: Importing model step file in Ansys Design Modeler

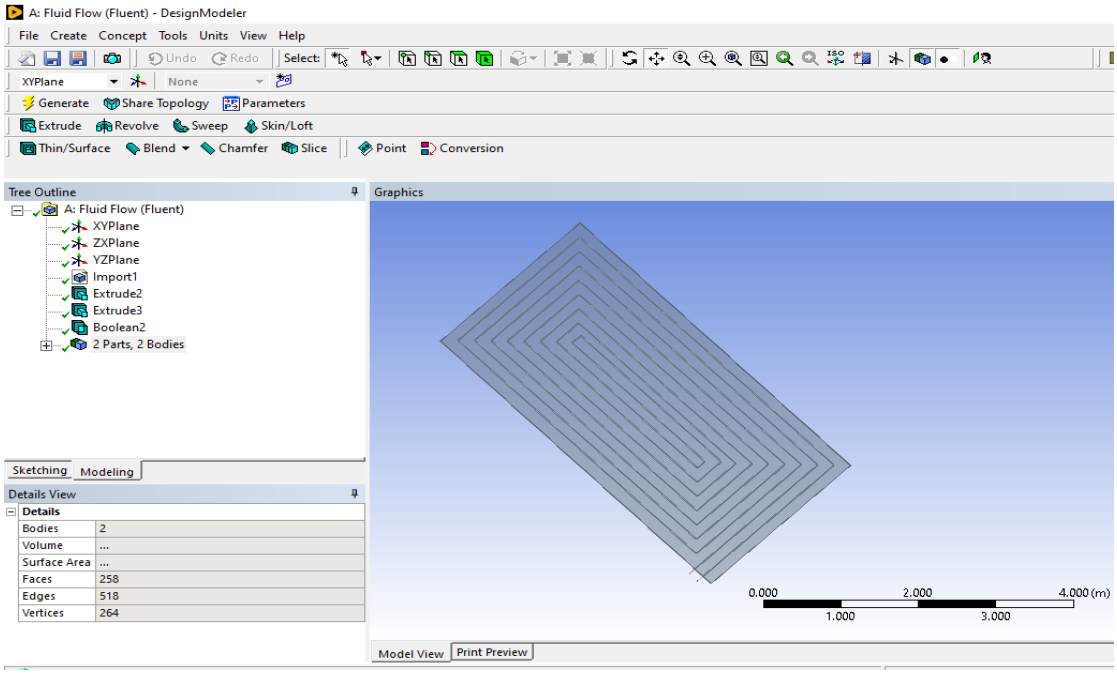


## Step 3: Mesh Generation of model in ANSYS

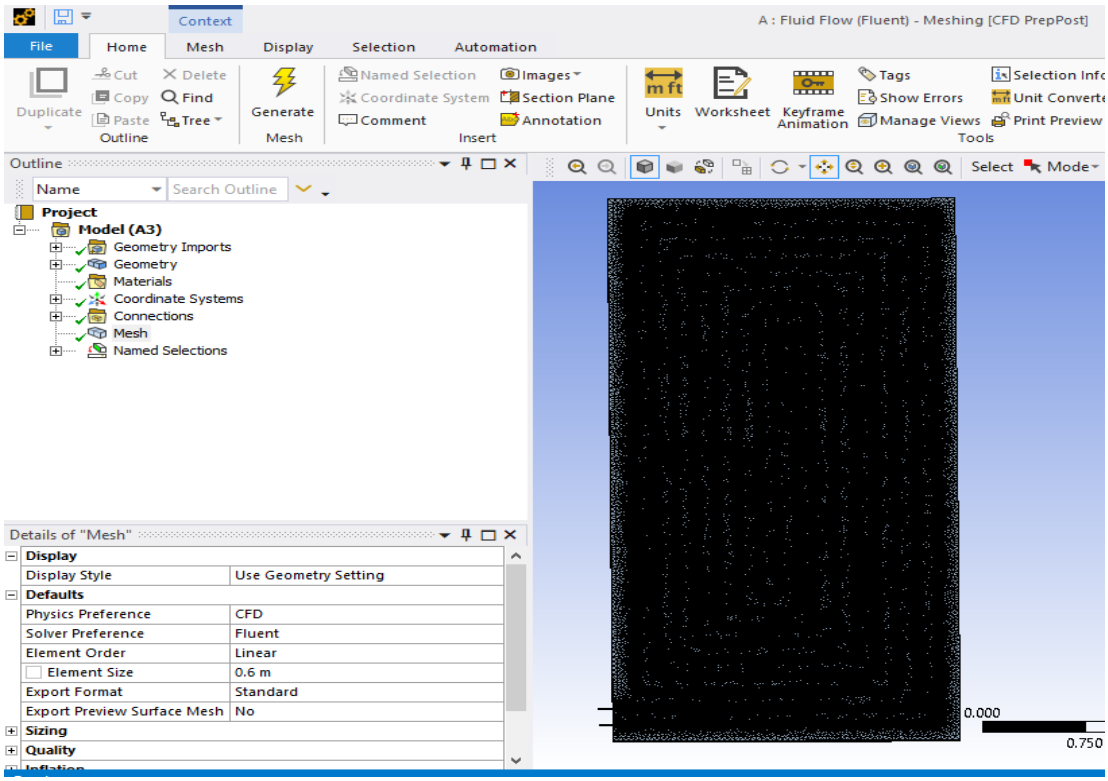

`

## Step 4: Setting Up boundary condition and solution setup

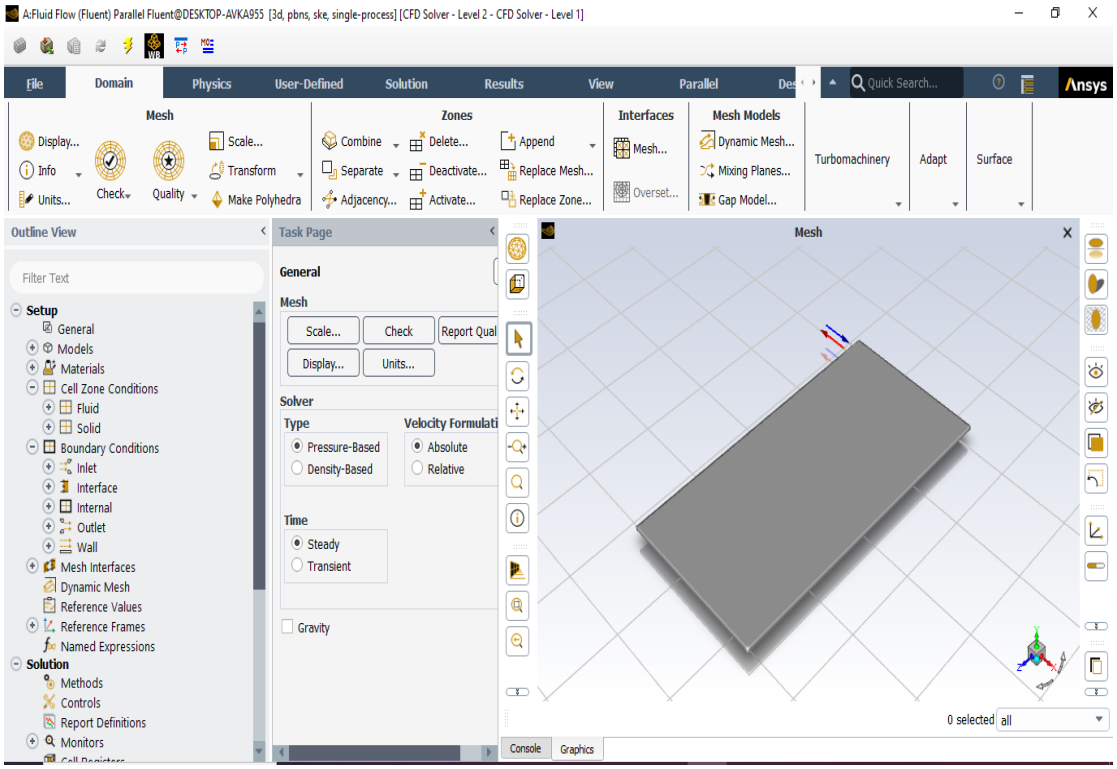


## Step 5: Post processing

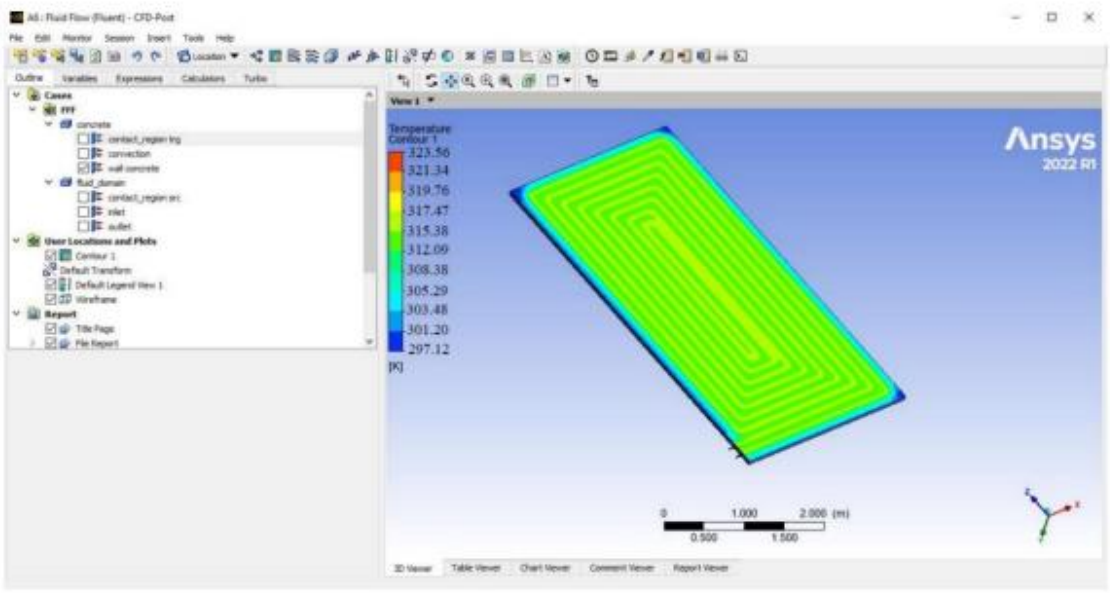

`

## APPENDIX B: OUTLET TEMPERATURE GRAPH

### Outlet Temperature for Offset Serpentine layout

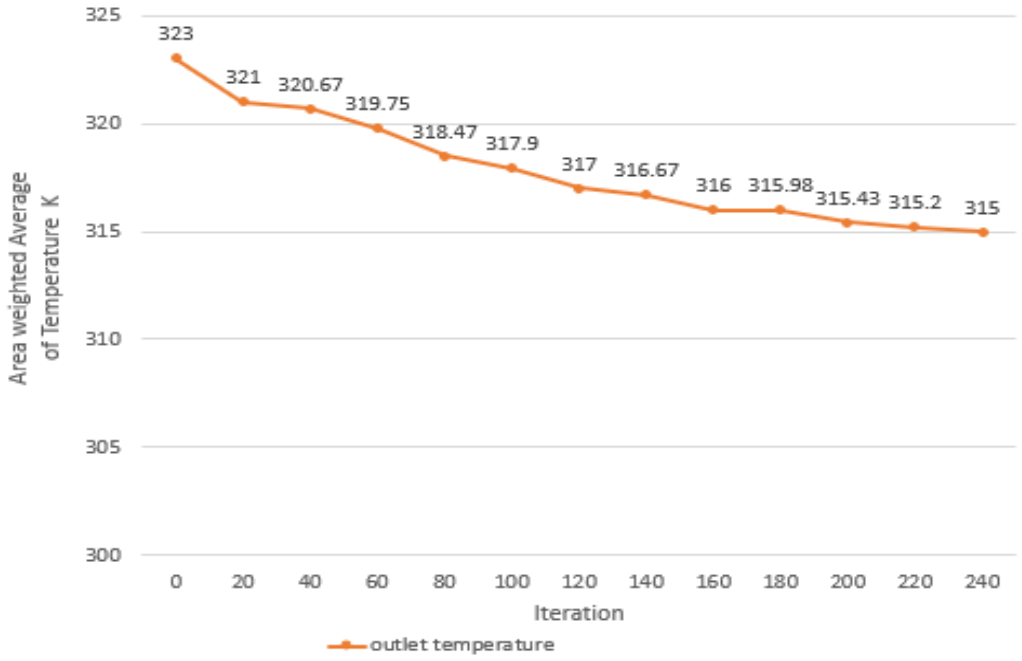


### Outlet Temperature for Counterflow layout

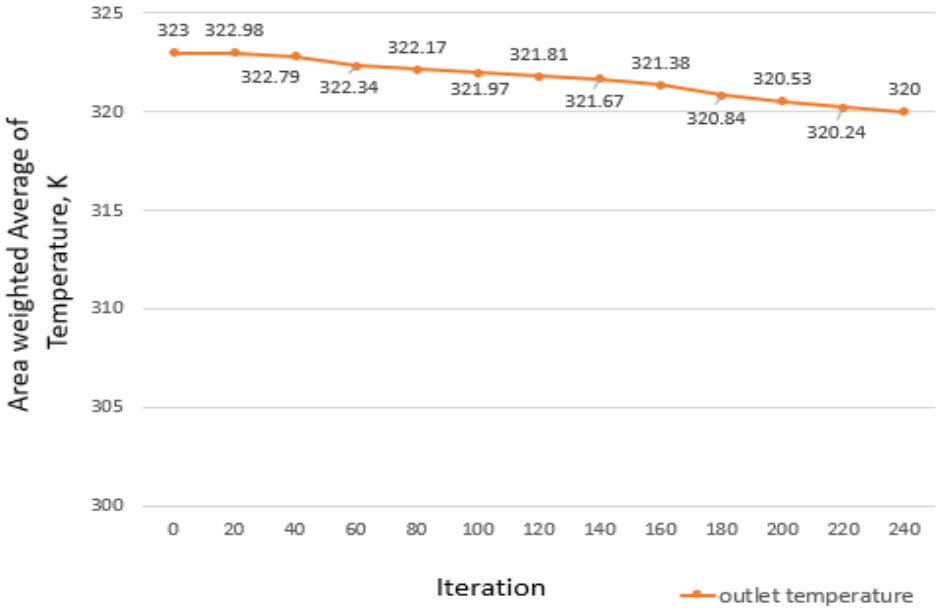

`

**Outlet Temperature for Counterflow layout with different inlet position**

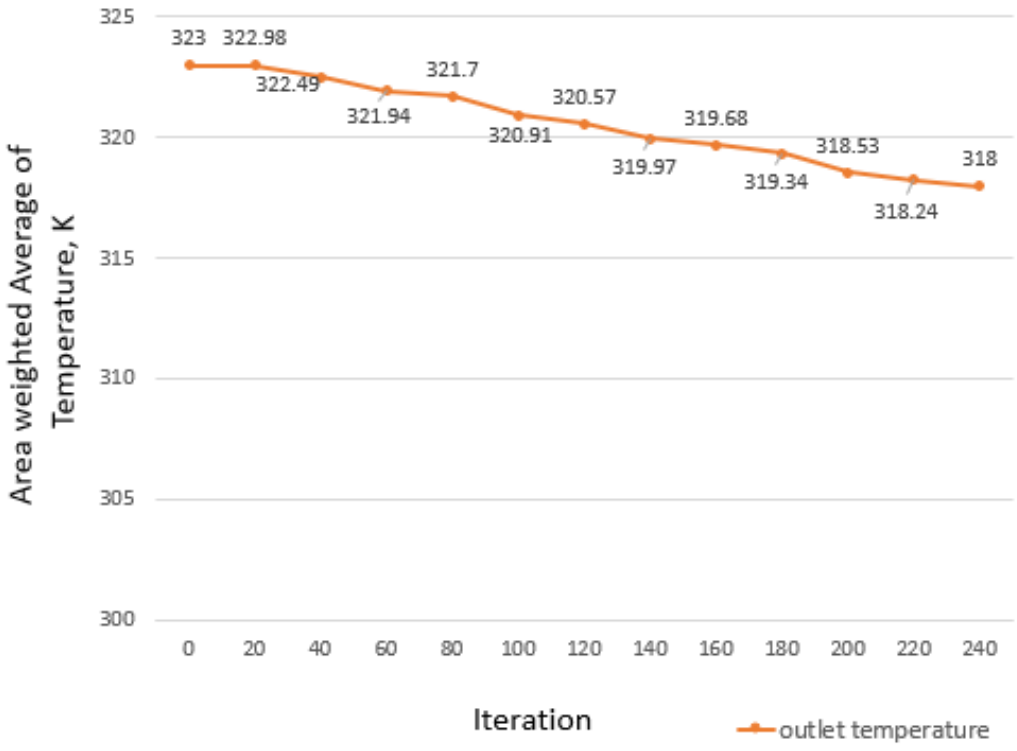

`

# Analysis of bend radius and inlet pipe position on hydronic radiant underfloor heating system

ORIGINALITY REPORT

13%
SIMILARITY INDEX

PRIMARY SOURCES

| | | |
|---|---|---|
| 1 | dokumen.tips<br>Internet | 47 words — 1% |
| 2 | Yinghui Wang, Xuelai Zhang, Jun ji, Zhen Tian, Yuyang Li. "Numerical Simulation of Thermal Performance of Indoor Airflow in Heating Room", Energy Procedia, 2019<br>Crossref | 46 words — 1% |
| 3 | wikimili.com<br>Internet | 42 words — 1% |
| 4 | Ngo, C. C., B. A. Alhabeeb, and M. Balestrieri. "Experimental Study on Radiant Floor Heating System", Volume 8A Heat Transfer and Thermal Engineering, 2015.<br>Crossref | 40 words — 1% |
| 5 | Tianying Li, Abdelatif Merabtine, Mohammed Lachi, Nadia Martaj, Rachid Bennacer. "Experimental study on the thermal comfort in the room equipped with a radiant floor heating system exposed to direct solar radiation", Energy, 2021<br>Crossref | 37 words — 1% |
| 6 | Monteiro, Joaquim Fernandes. "Experimental and Numerical Study on the Evaluation of Ventilation | 36 words — 1% |

Efficiency", Instituto Politecnico do Porto (Portugal), 2022
ProQuest

| | | |
|---|---|---|
| 7 | elibrary.tucl.edu.np<br>Internet | 36 words — 1% |
| 8 | Tri Ratna Bajracharyaa, Rabindra Nath Bhattaraiai, Sarika Kumari Mishra, Ashesh Babu Timilsina. "Variable Refrigerant Flow (VRF) System for Space Heating: A Case Study of Resort", Journal of the Institute of Engineering, 2018<br>Crossref | 33 words — 1% |
| 9 | innovativebuildingmaterials.com<br>Internet | 27 words — 1% |
| 10 | www.bdcnetwork.com<br>Internet | 26 words — 1% |
| 11 | elearning.unipd.it<br>Internet | 21 words — 1% |
| 12 | open.library.ubc.ca<br>Internet | 21 words — 1% |
| 13 | dspace.alquds.edu<br>Internet | 17 words — < 1% |
| 14 | core.ac.uk<br>Internet | 16 words — < 1% |
| 15 | Wang, Dengjia, Chunjin Wu, Yanfeng Liu, Penghao Chen, and Jiaping Liu. "Experimental study on the thermal performance of an enhanced-convection overhead radiant floor heating system", Energy and Buildings, 2017.<br>Crossref | 15 words — < 1% |

| | | |
|---|---|---|
| 16 | energy5.com<br>Internet | 13 words — < 1% |
| 17 | www.performanceengineering.com<br>Internet | 12 words — < 1% |
| 18 | Alshenaifi, Mohammad Abdullah Saud. "Optimising the Performance of Passive Downdraught Evaporative Cooling (PDEC) Towers for Saudi Housing: Investigating the Impact of Architectural Form", The University of Liverpool (United Kingdom), 2023<br>ProQuest | 9 words — < 1% |
| 19 | Jeetika Malik, Ronita Bardhan. "Thermal comfort perception in naturally ventilated affordable housing of India", Advances in Building Energy Research, 2021<br>Crossref | 9 words — < 1% |
| 20 | S. Oubenmoh, A. Allouhi, A. Ait Mssad, R. Saadani, T. Kousksou, M. Rahmoune, M. Bentaleb. "Some particular design considerations for optimum utilization of under floor heating systems", Case Studies in Thermal Engineering, 2018<br>Crossref | 9 words — < 1% |
| 21 | Giuliano Dall'O'. "Green Energy Audit of Buildings", Springer Science and Business Media LLC, 2013<br>Crossref | 8 words — < 1% |
| 22 | Progress in Clean Energy Volume 2, 2015.<br>Crossref | 8 words — < 1% |
| 23 | corpus.ulaval.ca<br>Internet | 8 words — < 1% |
| 24 | dokumen.pub<br>Internet | 8 words — < 1% |

25 nottingham-repository.worktribe.com
Internet

8 words — < 1%

| | | | |
|---|---|---|---|
| EXCLUDE QUOTES | ON | EXCLUDE SOURCES | < 6 WORDS |
| EXCLUDE BIBLIOGRAPHY | ON | EXCLUDE MATCHES | OFF |